

# An Analytic Mathematical Model to Explain the Spiral Structure and Rotation Curve of NGC 3198

Bruce Rout  
Cameron Rout

## Abstract

PACS:98.62.-g An analytical model of galactic morphology is presented. This model presents resolutions to two inter-related parameters of spiral galaxies: one being the flat velocity rotation profile and the other being the spiral morphology of such galaxies. This model is a mathematical transformation dictated by the general theory of relativity applied to rotating polar coordinate systems that conserve the metric. The model shows that the flat velocity rotation profile and spiral shape of certain galaxies are both products of the general theory. Validation of the model is presented by application to 878 rotation curves provided by Salucci, and by comparing the results of a derived distance modulus to those using Cepheid variables, water masers and Tully-Fisher calculations. The model suggests means of determining galactic linear density, mass and angular momentum. We also show that the morphology of NGC 3198 is congruent to the geodesic of a rotating reference frame and is therefore gravitationally viscous and self bound.

## 1 Introduction

An examination of previous studies of galactic rotation curves and morphology shows that, although relativistic effects of accelerating reference frames have been investigated, no integral resolution to theoretical discrepancies has been found. The special relativistic effects of material in orbit about the center of a galaxy appear to be negligible since the tangential velocity of such stars have been measured as moving at non-relativistic speeds. Nevertheless, it can be shown that general relativistic effects, as a result of centripetal acceleration, are significant and mask the measure of tangential velocity. Tangential velocities of stars in galaxies are measured using the shifting of spectral lines. This shifting is assumed to be strictly a Dopplerian effect. However, general, as well as special, relativistic analysis show that the shifting of spectral lines within rotating bodies are affected by both Doppler shift and effects of centripetal acceleration.

Historically, Keplerian rotational dynamics have been assumed in examining spiral galaxies. The observed tangential velocity of matter does not match a Keplerian model. This has resulted in the inference of significant amounts of non-luminous matter being required for a Keplerian model to match observed orbital behavior of galaxies as portrayed in rotation curves. To illustrate, an example of a rotation curve can be seen in Figure 1 which shows work by Begeman (1989) using the luminosity curve of NGC 3198 to calculate the expected rotation profile assuming Keplerian dynamics in comparison with measured values.

Two propositions which have resulted from the discrepancy between the expected and the observed rotation curves of galaxies such as NGC 3198 are: first, that more mass must exist within the system than appears in order for Keplerian dynamics to apply; second, that some new hypothesis on the laws of gravitational dynamics exists in lieu of Kepler's laws (Kepler, 1619). This paper demonstrates that existing scientific theories can explain the orbital behavior of galaxies without requiring assumptions of either additional mass or undiscovered gravitational principles. This is done by refuting that galaxies behave as though they consist of non-interacting particles of zero viscosity orbiting a central massive body; rather, that they consist of interacting orbiting bodies to which relativistic considerations must be applied. A resolution is presented here in the form of an analytical model which is a mathematical spiral having a flat rotation profile resulting from the application of Lorentz transformations in an accelerating environment.

## 1.1 Some Previous Approaches

A comprehensive overview examining the spiral structure of galaxies was done by Binney & Tremaine (2008). In this work, Binney assumes a non-viscous Keplerian model, provides extensive substantiation that spiral galaxies are indeed spirals at all wavelengths, and laments the lack of a complete exposition: "despite much progress, astronomers are still groping towards this goal," he writes. He presents a model of spiral morphology of galaxies based on a proposition of tidal forces generated by density waves. He rejects a model of stationary spiral structure and utilizes a rotating coordinate system. We present here a model in which a Keplerian non-viscous assumption is replaced by a general relativistic, highly viscous model also utilizing a rotating coordinate system. Furthermore, a similar consequence is found in which the metric, resulting from a rotating polar coordinate system, rather than density waves, creates a model having a stable rotating spiral structure of material.

Cooney et al. (2012) attempted to resolve the discrepancy between Keplerian motion and observed line width profiles through a general relativistic approach that used the Schwarzschild solution to constrain the metric with some success. Menzies & Mathews (2006) investigated and criticized a different model presented by Cooperstock & Tieu (2005) which, along with Gallo, & Feng (2010), utilized gravitational fields and associated curvature in the field equations balanced against Dopplerian Lorentz transformations in order to

obtain flat velocity curves of galaxies both numerically and analytically. Menzies showed this approach resulted in requiring an infinite amount of mass. These previous approaches show that the study of galactic structure and underlying physical models is still ongoing.

## 1.2 Galaxies as Non-Keplerian Systems

To apply the laws dictated by Kepler, the system must behave as a central massive region around which particles orbit without significantly interacting with each other, such as in the solar system. A useful description for such a system is provided by Zwicky as having negligible gravitational viscosity, or “zero-viscosity”. If the distribution of matter in a galaxy were such that the gravitational viscosity was not negligible, but rather high enough to “equalize the angular velocity throughout such systems regardless of the distribution of mass” Zwicky (1937), then such a galaxy would no longer be comprised of a central disc rotating with orbiting zero-viscosity matter.

Galaxies have a bright, dense central region with a sparse outer disc. Such a luminosity distribution suggests galaxies should behave as a zero-viscosity Keplerian system as modeled by Begeman (see Figure 1). However, observations by Begeman, Mathewson et al. (1992) and Persic et al. (1995) have shown that orbital velocities do not behave accordingly. We shall show that this discrepancy can be resolved by applying general relativistic effects and comparing it to observation. It is important to note that special relativistic effects apply to inertial reference frames and general relativistic effects apply to accelerating reference frames which include rotating bodies. This is especially relevant to deriving an analytical model of galaxies because general relativity, rather than special relativity alone, must be applied to rotating bodies since they are not inertial reference frames. For example, measuring the shifting of spectral lines in a heavily curved space, such as in the proximity of a black hole, must take into account the shifting of spectral lines independently of any object’s velocity. Similarly, space can be heavily curved in a galaxy, due to centripetal acceleration, which is also independent of the measured velocity of member stars. .

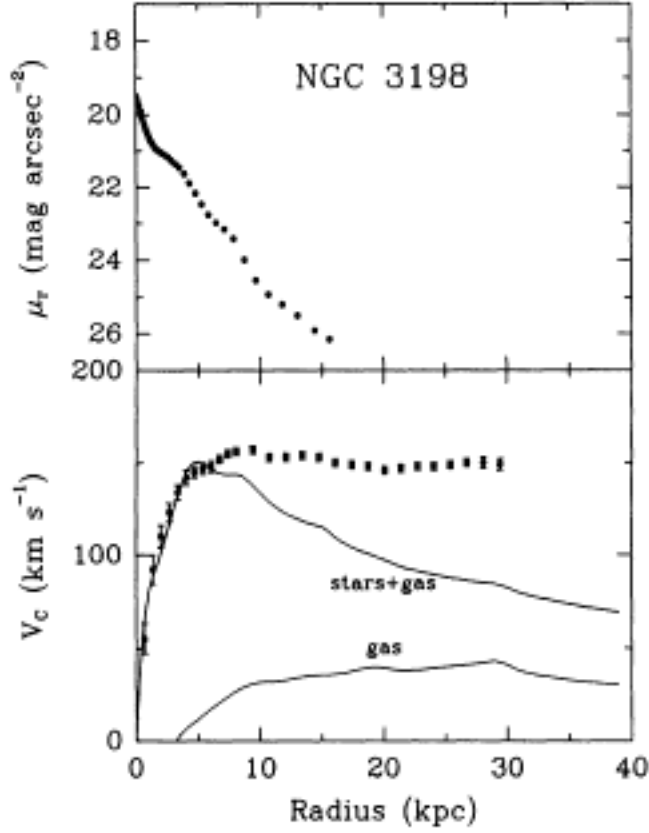


Figure 1: Begeman's plot of observed rotation velocities (bottom) compared with rotation curve predicted from the photometric data (top) assuming a constant mass-luminosity ratio and z-thickness. Begeman used a sech-squared law with disk thickness of  $0.2 \times$  the disk scale length and included the contribution of the gas component.

## 2 Relativistic Galactic Model

Restricting ourselves to a mathematical approach, wherein we retain the constancy of measures of the speed of light from the physical world, a model is derived using a measure in four dimensions. Comparisons can then be made of measures of length and time between coordinate systems which are moving and accelerating relative to each other. Consider two four-dimensional Minkowski spaces in which exist standard clocks and rulers at all points. We may compare the behavior of these clocks and rulers through various transformations

which conserve the metric, keeping the measure of the speed of light constant through each transformation. We may then transform measures into an appropriate coordinate system which shall prove useful in determining properties of spiral galaxies.

We derive the metric of a rotating body from Einstein et al. (1923) by considering the shape of a geodesic in a rotating system using Lorentz transformations.

Two important properties of a radial geodesic in a rotating coordinate system are as follows:

Firstly, the tangential velocity of such a coordinate system behaves peculiarly as a function of distance from the center. A relativistic model must take into account the fact that the tangential speed of a rotating coordinate system must never reach the speed of light. It is shown that the measure of tangential velocity reaches a limit as distance from the center of rotation increases.

Secondly, the path of light traveling radially outward from the center of rotation traces a spiral-shaped path within the rotating coordinate system. More specifically, it approaches an Archimedes' Spiral, defined as a spiral having a constant pitch. The pitch,  $\kappa$ , of an Archimedes' spiral in polar coordinates is analogous to the slope of a straight line in Cartesian coordinates. That is:

$$r = \kappa\theta \tag{1}$$

as compared to

$$y = mx \tag{2}$$

where  $r$  is radial distance from the origin,  $\theta$  is the angle subtended anti-clockwise from the x-axis,  $\kappa$  is a constant;  $x$  and  $y$  are the usual x-y coordinates and  $m$  is the slope of a straight line – a constant. These equations are well known and are presented in the general sense to show similarity in form.

We first show the effect of a strictly mathematical transformation of pixels of a digital image from one coordinate system to another. Following this, we examine the effects of general relativity in rotating coordinate systems which result in these transformations.

## 2.1 A Spiral Transformation

We present an analytic model in which the distinct spiral shape of galaxies appears asymptotically as a function of distance from the center. Following which, we show how it can determine certain galactic parameters which are of interest. Please note that the resultant model of spiral galaxies is not a pure Archimedes' Spiral but uses the morphology of an Archimedes' Spiral as an asymptote to which the shape of spiral galaxies quickly approaches as a function of radial distance depending on their rate of rotation. This model is applicable to galaxies which have a distinct flat rotation profile; galaxies which do not have flat velocity profiles would deviate from this model.

The following equations determine a transformation which is applied to the pixels of an elongated blob as in Figure 2 (left).

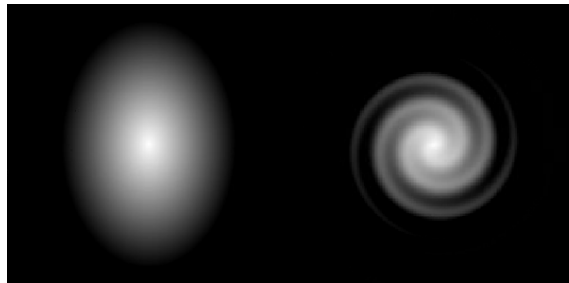


Figure 2: The left figure is an elongated blob of white against a black background in Cartesian coordinates with the origin at the center of the figure while the figure on the right is the transformation of the left figure using Equations (3) and then portrayed on an orthogonal rectilinear grid. The transformation used a value of  $\kappa = 20$ .

Consider the following spiral transformation:

$$\begin{aligned}
 r &= \sqrt{x^2 + y^2} \\
 \theta &= \arctan(y/x) \\
 r' &= r \\
 \theta' &= \theta - r/\kappa \\
 x' &= r' \cos(\theta') \\
 y' &= r' \sin(\theta')
 \end{aligned} \tag{3}$$

where  $x$  and  $y$  are the coordinates of a particular pixel in the originating figure with the origin at the center.

The first two equations in the transformation of Equations (3) transform the pixels of a figure into polar coordinates. The second two transform the pixels onto a spiral rotation while the last two transform the results into Cartesian coordinates and can be portrayed as rows and columns of a resultant figure. Note that Figure 2 (right), is a shape resembling a spiral galaxy. This mathematical transformation results in a figure which shows a distinct spiral morphology even though the original figure is somewhat amorphous. The units used in the transformation are pixel-length units with the origin of both polar and Cartesian coordinates at the centre of the blob and spiral shape respectively. A pixel smoothing software was used following the transformation to eliminate gaps in the resultant spiral and the pixel brightness following the transformation is therefore slightly altered.

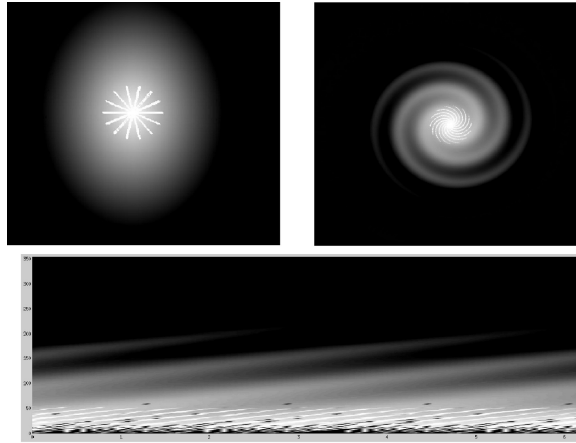


Figure 3: The top left figure is an elongated blob with bright radial structure at the center. This blob is then transformed with a rotation in the upper right figure. The upper right figure is then portrayed in rectilinear coordinates with  $r$  as the ordinate and  $\theta$  the abscissa and shown in the lower figure. The lines in the lower figure slope to the right as a result of the clockwise “spin” of the upper right figure.

The superimposition of a star shape at the center of an oval cloud is shown in Figure 3 (upper left). The spiral transformation described by Equations (3) is applied to the pixels in this figure and then shown in Figure 3 (upper right). This figure also has a clearly defined spiral morphology including the brighter, smaller spirals in the middle of the figure. Figure 3 (lower) is a portrayal of the upper right figure with the ordinate as  $r$  and abscissa as  $\theta$ . The series of parallel straight lines and their slope denote a value of  $\kappa = 20$ , which was used in the transformation.

This is a very “powerful” transformation in that an original figure, which may resemble nothing more than something akin to a slightly elongated blob, resembles a distinct spiral following this transformation. The analytic model which follows shows that the general theory of relativity, due to the acceleration of circular motion, compels this transformation. Therefore, the mathematical transformation demanded by the general theory of relativity, rather than the morphology of material being so transformed, results in both the spiral morphology of certain galaxies and their flat rotational velocity profile. This is demonstrated in the following sections.

## 2.2 Comparison of the Spiral Transformation to Some Spiral Galaxies

For a given spiral such as in Figure 3 (upper right), consider mapping  $r$  onto  $y$  and  $\theta$  onto  $x$ , in order to observe a possible linear orientation. This results in a measure of  $\kappa$ , equal to the slope of bright parallel lines in Figure 3 (lower).

Continuing,  $\kappa$  was measured for three different galaxies as shown in Figures 4-6. In these figures, the position of each photograph's pixel is transformed from a row-column coordinate to polar coordinates in which the center of the galaxy is the origin,  $r$  is the distance in pixels from the center of the galaxy and  $\theta$  is the angular measure from a horizontal axis as in polar coordinates. The position of these pixels are then transformed where  $r$  is the ordinate and  $\theta$  the abscissa. In these figures, Equation 1 is investigated by inspecting the linear orientation of the resultant pixel greyscales.

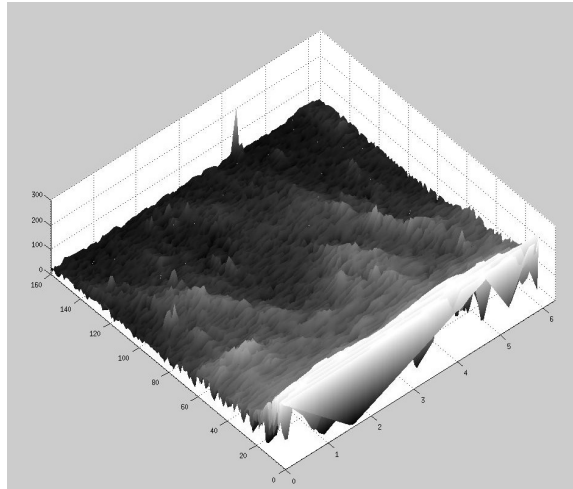


Figure 4: A three dimensional luminosity figure of NGC 4321 where  $\theta$  is the abscissa and radial distance from the center of the galaxy is the ordinate. Note the linear orientation of luminosity elevations in the figure which correspond to the spiral arms of the galaxy. Also note the spate of flocculence near the center of the galaxy is also oriented linearly with the same slope. The linear ridges appear parallel and encourage the derivation of Equation (20) from physical parameters.

Note the three dimensional representation of luminosity vs.  $r$  and  $\theta$  of NGC 4321 in Figure 4. In this figure there are two obvious linear ridges of greater luminosity oriented with consistent negative slope emanating from the abscissa and separated by  $\pi$  radians. Also in this figure there are other shorter ridges and peaks emanating from the abscissa with similar slope. In Figure 7, also portraying NGC 4321,  $\kappa$  is approximated to be -32 pixels per radian which is the value of the slope of the two lines superimposed on the figure.



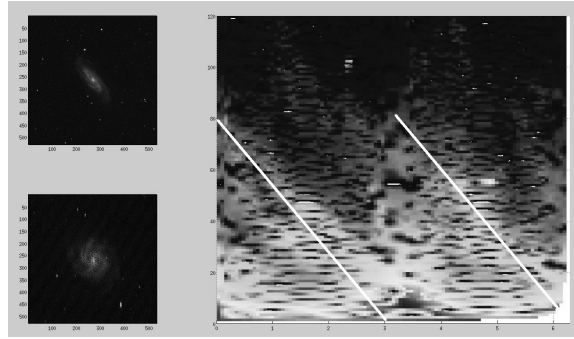


Figure 5: This is a portrayal of a digital photograph of NGC 3198 with the original photograph on the upper left, a transformation of the pixels of the galaxy so that the galaxy appears as viewed from directly above on the lower left and a transformation of the lower left photograph, transforming the pixels of the photograph into a plot of radial distance from the center of the galaxy vs.  $\theta$  as per polar coordinates, on the right. Note in the transformed photograph on the right, the two bright linear orientations of lighter shades are parallel and a horizontal distance of  $\pi$  radians from each other with a slope of -26 pixels per radian.

The galaxy NGC 4321 is oriented with a small angle of incline. As a result, the above described transformation can be conducted without requiring alteration, which is portrayed in Figures 4 and 7. However, we examine NGC 3198 in Figure 5 by first correcting for the angle of incline as shown in the figures on the left and then applying the above described transformation, the results of which are shown on the right of the figure. From this figure we can estimate a value for  $\kappa$  of -26 pixels per radian.

IC 239 is also a distinct spiral galaxy with a small angle of incline. Figure 6 is a result of the above transformation in which a value of -11 pixels per radian can be estimated as a value of  $\kappa$  in a spiral equation approximating the distribution of luminosity for this galaxy.

These observed properties can be explained through general relativistic considerations.

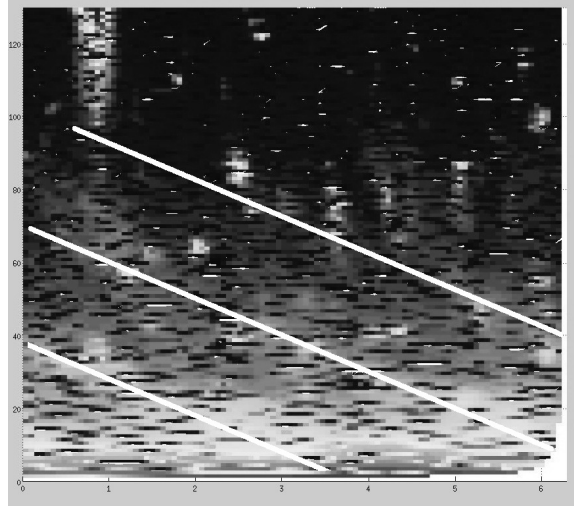


Figure 6: This is a portrayal of a digital photograph of IC 239 as a result of transforming the pixels of the photograph into a plot of radial distance from the center of the galaxy vs.  $\theta$  (as per polar coordinates). Note the prominent linear orientations of bright pixels are parallel and a horizontal distance of  $\pi$  radians from each other. These lines have a common slope of approximately -11 pixels per radian. The line on the far left continues on the right. The lines overlay areas of greater luminosity and mark the positions of the two spiral arms emanating from the center of the galaxy.

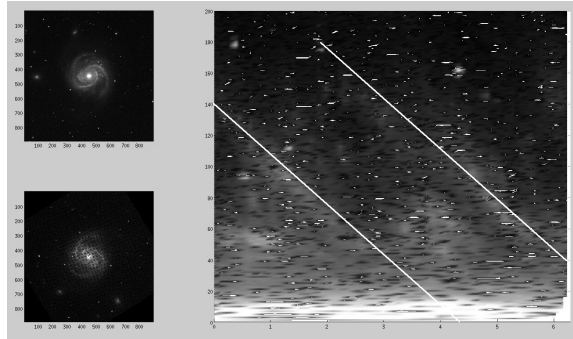


Figure 7: This is a portrayal of a digital photograph of NGC 4321 (upper left), a rotation of the photograph (lower left) and the result of transforming the pixels of the photograph into a plot of radial distance from the center of the galaxy vs.  $\theta$  as per polar coordinates (right). Note the two distinct bright linear orientations of higher luminosity which have been overlaid by straight lines in the figure on the right. These lines are parallel and a horizontal distance of  $\pi$  radians apart and have a common slope of -32 pixels per radian.

### 2.3 Lorentz Transformations in a Rotating Coordinate System

The Lorentz factor between two coordinate systems moving with instantaneous velocity,  $v$ , relative to each other is:

$$\gamma = \frac{1}{\sqrt{1 - v^2/c^2}}. \quad (4)$$

If  $v$  is a constant then the Lorentz factor can be applied according to well-known special relativity. However, if two coordinate systems are accelerating relative to each other, then  $v$  is not a constant and the Lorentz factor is a variable. In such a case, equation (4) can only be applied for an instant.

The model presented uses the coordinate systems, reference frames, and application of Lorentz foreshortening in a rotating system as described by Einstein, in the following quote:

In a space which is free of gravitational fields we introduce a Galilean system of reference  $K(x, y, z, t)$ , and also a system of co-ordinates  $K'(x', y', z', t')$  in uniform rotation relatively to  $K$ . Let the origins of both systems, as well as their axes of  $Z$  permanently coincide. For reasons of symmetry it is clear that a circle around the origin in the  $X, Y$  plane of  $K$  may at the same time be regarded as a circle in the  $X', Y'$  plane of  $K'$ . We suppose that the circumference and

diameter of this circle have been measured with a unit measure infinitely small compared with the radius, and that we have the quotient of the two results. If this experiment were performed with a measuring-rod at rest relatively to the Galilean system  $K$  then the quotient would be  $\pi$ . With a measuring rod at rest relatively to  $K'$ , the quotient would be greater than  $\pi$ . This is readily understood if we envisage the whole process of measuring from the “stationary” system  $K$ , and take into consideration that the measuring-rod applied to the periphery undergoes a Lorentzian contraction, while the one applied along the radius does not. Einstein et al. (1923)

Consider two polar coordinate systems having coincident origins, one is not rotating and is denoted as the  $K$  system, the other is rotating with some angular velocity  $\omega_0$  as measured by  $K$  and is denoted as  $K'$ . We transform the coordinates of the  $K'$  system into the coordinates of the  $K$  system.

The influence of gravity follows a geodesic. Thus, the shape of a geodesic can be transformed from  $K'$  to  $K$ .

Consider further the behavior of two identical clocks, one in the  $K$  system and the other rotating in the  $K'$  system at coincident points. The clock in the  $K'$  system will be a slower clock as measured by the one in the  $K$  system. This effect is more pronounced at other coincident points further from the origin of the two systems. Therefore the Lorentz factor describing this effect will not be a constant throughout the systems and will vary as a function of  $r$ , the distance from the origin. Since the Lorentz factor is not a constant, General Relativistic effects, rather than Special Relativistic effects, need to be applied.

Because clocks in  $K$  and  $K'$  measure the passage of time differently, the period of rotation of the  $K'$  system will be different than that measured by clocks in the  $K$  system. Although all clocks in the  $K$  system will measure the  $K'$  period of rotation the same, say some value  $T_0$ , the clocks in the  $K'$  system will measure variable periods of rotation and this period will vary as a function of  $r$  due to the differing tangential velocities of points in  $K'$  also being a function of  $r$ . Let us denote the period of revolution of  $K'$  as measured by clocks in  $K'$  as  $T'(r)$ . The ratio of  $T_0/T'(r)$  is the Lorentz factor by definition and we shall denote this variable Lorentz factor as  $\gamma(r)$ .

It follows that,

$$\gamma(r) = \frac{T_0}{T'(r)} \quad (5)$$

as above. If we denote the angular velocity as  $\omega_0$  as measured in  $K$  and  $\omega'(r)$  as measured in  $K'$ , we therefore have:

$$\begin{aligned}
\omega'(r) &= \frac{2\pi}{T'(r)} \\
\omega_0 &= \frac{2\pi}{T_0} \\
\omega'(r) &= \frac{\omega_0}{\gamma(r)}.
\end{aligned} \tag{6}$$

Please note that identical rulers differ in their measures in the two systems. Rulers in  $K'$  will be foreshortened in the tangential direction relative to  $K$ . The rulers will be identical if oriented in the radial direction. Of course the measure of the tangential velocity in both systems would be identical at coincident points provided one was consistent in using the same clocks and rulers restricted to the system in which the tangential velocity is being measured. Here also, care must be taken to define tangential velocity as arc length traversed over time. It will be shown that the variation of the Lorentz factor, based on differences in the measure of angular velocities, that is  $\omega'(r)$  and  $\omega_0$ , will affect the difference in measures of shifts in spectral lines. This effect could possibly be compared to that of curvature, however, in the opposite sense of curvature described by the Schwartzchild metric in gravitational fields. In a gravitational field, the Lorentz factor increases closer to the source of the field, in a rotating system such as  $K'$ , the Lorentz factor increases further from, rather than closer to, the center of rotation.

Returning to our presentation of transformations between  $K'$  and  $K$ , please consider the following well known equation for circular motion in general:

$$v = \omega r. \tag{7}$$

where we usually consider  $v$  as tangential velocity in a rotating system,  $\omega$  as the angular velocity, and  $r$  as radial distance. This is a general case without considering relativistic effects and well known since the time of Galileo. However, in the case of a rigid body,  $\omega$  is a constant; in the case of a rotating coordinate system which conserves the metric, the angular velocity is a variable and is denoted here as  $\omega'(r)$ . As soon as we bring in the effects of the differences in clocks and rulers between  $K'$  and  $K$ , we deviate from classical, or Newtonian, rotational dynamics. Care must be taken in the transformations from one system to the other.

Consider some distance  $r$  from the coincident origin in both systems as a parameter. At each parametric  $r$ , and for some very small moment of time, at two coincident points in  $K'$  and  $K$  some distance  $r$  from the coincident origin,

$$v'(r) = \omega'(r)r, \tag{8}$$

where  $v'(r)$  and  $\omega'(r)$  are tangential velocity and angular velocity as measured in  $K'$ ; then, parametrically,

$$\gamma(r) = \frac{1}{\sqrt{1 - v'(r)^2/c^2}}. \tag{9}$$

Then,

$$\gamma(r) = \frac{1}{\sqrt{1 - \omega'(r)^2 r^2 / c^2}}. \quad (10)$$

Substituting equation (6) we have:

$$\gamma(r) = \frac{1}{\sqrt{1 - \omega_0^2 r^2 / (\gamma(r)^2 c^2)}}. \quad (11)$$

Solving for  $\gamma(r)$  we have:

$$\gamma(r) = \sqrt{1 + \frac{\omega_0^2 r^2}{c^2}}. \quad (12)$$

This yields the spatially two-dimensional time dependent metric in  $K'$ ,

$$ds^2 = \frac{c^2}{\gamma(r)^2} dt^2 - dr^2 - \gamma(r)^2 r^2 d\theta^2. \quad (13)$$

We have used

$$g_{tt}^{-1} = g_{\theta\theta} = \left(1 + \frac{\omega_0^2 r^2}{c^2}\right) \quad (14)$$

where  $g_{\mu\nu}$  is the metric tensor in order to derive equation (13).

## 2.4 Equation of a Spiral Geodesic

The path of a photon traveling radially outward from the origin would travel in a straight line according to coordinates in  $K$  but would trace out an Archimedes' Spiral within  $K'$ . Furthermore, as the photon travels outwardly it passes over sections of  $K'$  whose local clocks and tangential distance measures deviate from those measured within  $K$ , according to the Lorentz factor as described in equation (12).

We see from equation (12) that a linear relationship between  $\gamma(r)$  and  $r$  begins to be established asymptotically at distances  $r > \frac{c}{\omega_0}$  from the center of the rotating system. As a result, the calculated tangential velocity using differences in spectral lines, which is effected by  $\gamma(r)$  would approach an asymptote which we denote as  $v_{max}$ .

### 2.4.1 Discussion of Units

In examining the metric of equation (13), and the equation for the Lorentz factor in equation (4), we see an interchangeability between time and space coordinates by either multiplying the time coordinate by the speed of light or by dividing spatial coordinates by the same value. Coordinates in a Cartesian Minkowski space are  $(ict, x, y, z)$ . Converting from a Minkowski space in MKS units to completely unit-less dimensions such as  $\tilde{R}$  for radial distance,  $\tilde{v}_{max}$  for the asymptote of tangential velocity and  $\tilde{\omega}_0$  for angular velocity we have:

$$\tilde{v}_{max} = \frac{v_{max}}{c}, \quad (15)$$

$$\tilde{r} = \frac{r}{c\tau}, \quad (16)$$

and

$$\tilde{\omega}_0 = \omega_0\tau \quad (17)$$

where  $\tau$  is the number of seconds in a year, assuming the original measurements are in MKS units and radians are considered unit-less.

For convenience one may consider  $\tilde{r}$  as the value of spacial measurement in ly and  $\tilde{\omega}_0$ , as a measure in radians per year.

The law of rigid bodies predicts a constant angular velocity throughout the entire rotating body. However, taking relativity into account, the measure of angular velocity varies with radial distance and yet the entire body appears rigid, or has a stable shape over time. The value of  $\tilde{\omega}_0$  is constant throughout the rotating coordinate system: however, the value of angular velocity,  $\omega'(r)$ , is not. As a result, the rotating coordinate system, although appearing as a set of rigid rotating spirals, would have different measures of  $\omega'(r)$  at various radial distances. This is contrary to the laws of a rigid body according to Newton's laws of motion or to Lagrangian mechanics which are based on non-relativistic considerations.

In general, the Lorentz factor is:

$$\gamma(r) = \sqrt{1 + \tilde{\omega}_0^2 \tilde{r}^2}. \quad (18)$$

The constant of proportionality between the radial coordinate and the orthogonal angular coordinate is  $2\pi$ . Therefore:

$$\tilde{\omega}_0 = \frac{\tilde{v}_{max}}{2\pi}. \quad (19)$$

Further than a distance of  $1/\tilde{\omega}_0$  from the center, the tangential velocity approaches a constant velocity,  $\tilde{v}_{max}$ . From this distance outward, on the plane of a revolving coordinate system, the equation of a radial spiral geodesic as measured in  $K'$  and transformed onto the coordinate system of a non-revolving observer is:

$$\tilde{r} = \frac{\theta}{\tilde{\omega}_0}. \quad (20)$$

## 2.5 Equation Describing the Flat Velocity Profile

Applying equation (12) to the measured tangential velocity using the shifting of spectral lines,  $v_{tan}$ , by a non-revolving observer, we now have:

$$v_{tan} = v_{max} \cdot \frac{\tilde{\omega}_0 \tilde{r}}{\sqrt{1 + \tilde{\omega}_0^2 \tilde{r}^2}}. \quad (21)$$

As  $\tilde{r}$  increases,  $v_{tan}$  approaches an asymptote for the maximum tangential velocity as determined by the effects of the Lorentz transformation, which we denoted as  $\tilde{v}_{max}$ , as a unit-less number, and as  $v_{max}$ , in equation (21). This completes the derivation of two important functions. One is equation (20), which is the equation of a spiral describing a geodesic in  $K'$ , and the other is equation (21), which describes the *apparent* tangential velocity of coordinates in  $K'$  calculated by measuring the shifting of spectral lines. We now apply these equations to observations of galaxies. Note that the value of  $v_{tan}$  is a measure of velocity using spectral lines and from relativistic effects has a different value than the tangential velocity denoting arc length traversed per unit time. Therefore  $v(r)$  of equation (7) is not the same as  $v_{tan}$ .

### 3 Flat Velocity Rotation Profiles

The flat velocity rotation curve of galaxies indicates that nearly all the stars within a galaxy appear to have the same tangential velocity. The model presented here shows this is caused by a discrepancy between the measure of tangential velocity using shifting of spectral lines and actual tangential velocity: that is, distance traveled divided by elapsed time. As a result, the measure of tangential velocities are well below relativistic speeds. In effect, the shifting of spectral lines does not measure the actual tangential velocity of stars within the galaxy.

#### 3.1 An Examination of the Rotation Curve of NGC 3198

The rotation curve of NGC 3198 is shown in Figure 8. We have curve-fitted equation (21) to the observations of Begeman and overlaid the result atop the observed values. The data points provided by Begeman have a reported error in rotational velocity of 5 km/s and an error in angular measure of 15'' of arc. The calculated fit, shown as a continuous line, has a normalized sigma of 0.04 from the data points provided and yields a fitted  $v_{max}$  of 152.9 km/s  $\pm$  3.78 km/s. We see that there is a significant correlation between observed values of the rotation curve and the presented model.

There are two parameters involved in obtaining the calculated fit. One is  $v_{max}$  and the other is an angular-distance ratio to couple the values given by Begeman in arcmin and the values used in equation (21) in ly. A linear regression was used where  $v^2/R_{arcmin}^2$  was the ordinate and  $v^2$  the abscissa.  $v$  is the measured tangential velocity in km/s and  $R_{arcmin}$  is the angular distance from the center of the galaxy in arcmin.

This ratio can also be used to estimate the distance to the galaxy although there is a fairly significant degree of allowable error. Fitting the data presented by Begeman, a distance of 19.2 Mpc was found. However, there are discrepancies and difficulties in



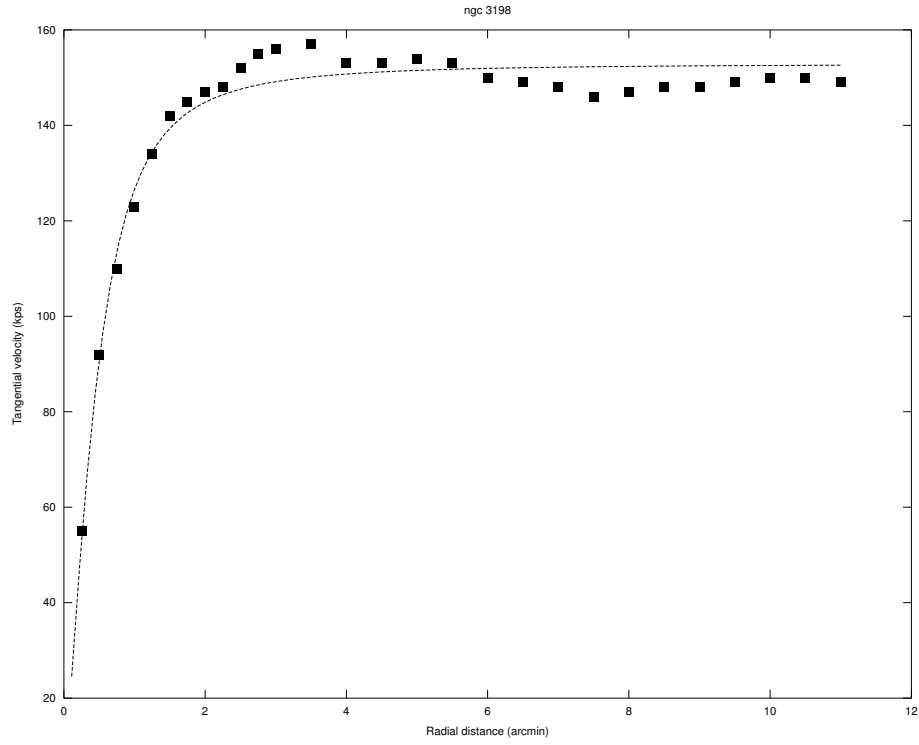
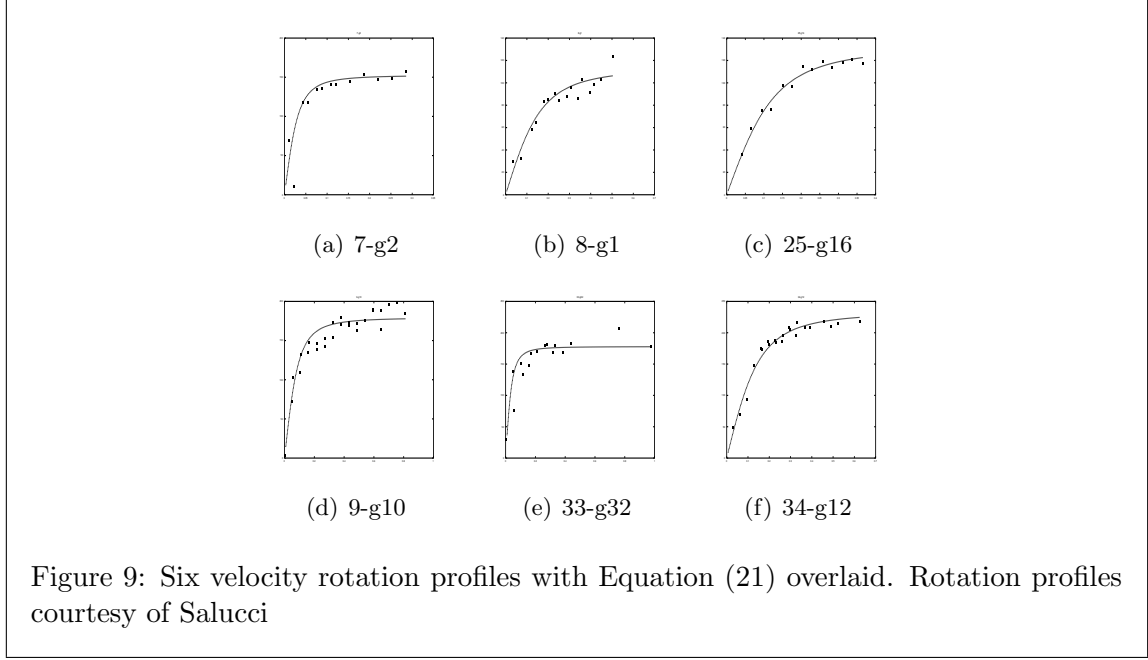


Figure 8: Begeman’s rotational data overlaid with a curve fit of equation (21). The fit yields a normalized sigma of 0.04 and a  $v_{max}$  of 152.9 km/s.

accurate measurements near the center of the galaxy. Uncertainties in radial measures are at about 15 arcsec as reported by Begeman. The beam width is 30 seconds of arc and the CLEAN software can remove about 1/3 of beam smearing. If the values of radial distance have a discrepancy of 10 seconds of arc, there is a variation in the measure of distance from 12.7 to 48.4 MPc. While (21) can give some indication of distance, the problems with finding the center of rotation, coupled with error allowances, near the center of the galaxy, involves a high degree of error. However, future work on improving methods of finding a more accurate distance modulus from rotation profiles may prove very fruitful.



### 3.2 Rotation Curves of 878 Galaxies

We have also applied equation (21) to 878 velocity rotation profiles from Salucci (Persic et al., 1995) to obtain an average normalized standard error of 0.0756 with a standard deviation of .049. (Some examples are shown in Figure 9).

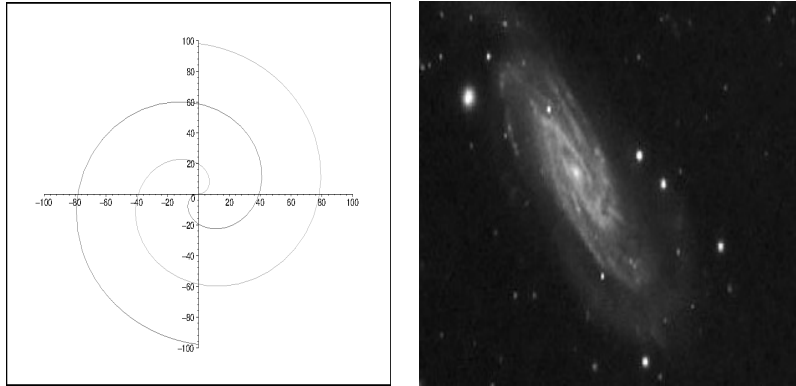
Table 3, at the end of this paper, lists these galaxies with the fitted  $v_{max}$  for each galaxy and the normalized  $\sigma$  of the fit of each galaxy's rotation curve to equation (21).

## 4 Spiral Morphology

The analytical model presented is simply a mathematical spiral as per Equation (20) with  $\omega_0$  being the constant angular velocity of the galaxy. Digital photographs from the MAST Digital Sky Survey with maximum response wavelengths between 6400 and 6700 ÅSTSI (2006) are used in further analysis. Note that the ratio of pixels to arcmin in photographs used is 1.008.

### 4.1 Spiral Morphology of NGC 3198

A  $v_{max}$  of 151 km/s for NGC 3198, as given by Begeman, was substituted into Equations (19) - (20). The resultant curve as described by a geodesic traced out on an equivalent rotating coordinate system to a photograph of the galaxy as in Figure 10 (b) was then



(a) A spiral generated from tracing (b) NGC 3198 in Ursa Major. NGC 3198 is classified SBc(R) Youman (2005). The scale is in thousands of light years.

Figure 10: A double-arm Archimedes' Spiral is shown in Figure 10(a) and a photograph of NGC 3198 is in Figure 10(b). There appears to be a morphological similarity between the two structures which suggests that an analytical model based on a spiral shape is possible in order to describe galactic morphology and parameters.

drawn. This curve is shown in Figure 10 (a). It is a graph of a double Archimedes' spiral which closely resembles the photo of NGC 3198. Note the scale of the graph is in thousands of ly as per equation (20). There appears to be a remarkable morphological similarity and a possibility of determining the intrinsic size of the galaxy itself.

## 4.2 Measuring the Spiral Pitch of NGC 4321

In the above description of a spiral transformation it can be seen that the resultant spiral shapes of material adhering to GR in rotating coordinate systems is a result of the transformation from one reference frame to another while conserving the metric. The spiral described by Equation (20) is valid for the region where the tangential velocity of material appears as a constant with respect to radial distance from the center of a rotating coordinate system. This becomes valid when  $r \gg 1/\omega_0$ . (Note,  $r$  is in units of ly and  $\omega_0$  is in units of radians per year). Thus the outer regions of a galaxy, where a constant rotation profile is well established, can be expected to manifest a constant pitch.

Figure 11 is a photo of NGC 4321 with a spiral overlaid according to Equation (20) using a value of -32.15 arcsec per radian as a value of  $\kappa$ . This approximates the well-defined spiral portion of NGC 4321. The resultant spiral of this pitch would have an arm spacing

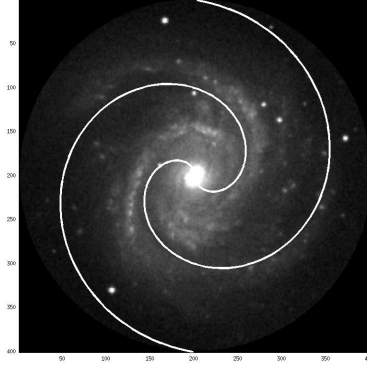


Figure 11: NGC 4321 with spiral overlays according to Equation (20) with a pitch of  $-32$  arcsec per radian. Note the outer portions of the spiral fall along the path of greater luminosity in the photo of the galaxy.

close to  $\pi \times 32$ , or about 100 pixels. Let us define arm spacing as the radial distance between distinct local maxima in the luminosity profile on a line taken through the center of the galaxy, viewing the galaxy as from above. This can be very accurately measured using an FFT of the luminosity along this line. If a galaxy is inclined on the celestial sphere, then this line would be oriented along the major axis of the galaxy for the measure of arm spacing to be valid. However, NGC 4321 is seen as a spiral galaxy from almost directly above and the arm spacing, as defined, would be very close to a constant for all cross-sections.

This was investigated by taking 360 luminosity cross sections through the center of the galaxy at half-degree intervals, applying an FFT along these cross sections, and examining the results to see if a value very close to 100 arcsec would appear. A consistent value of 100.99 arcsec presents itself with values of 134.42 and 80.81 arcsec above and below. This analysis is graphically shown in Figures 12 to 15.

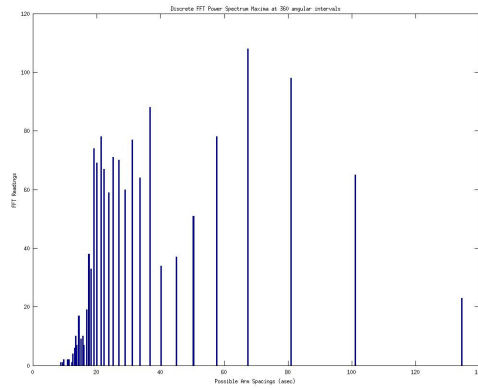
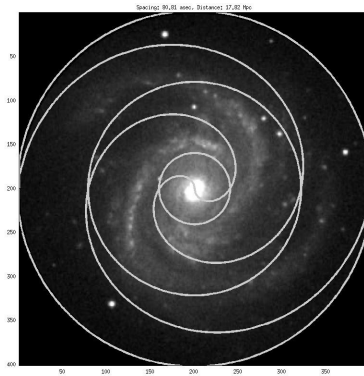


Figure 12: A histogram showing FFT values with different cross section orientations of NGC 4321. A distinct value of 100.99 arcsec can be seen. There are also distinct peaks at 80.81 and 134.42 arcsec.



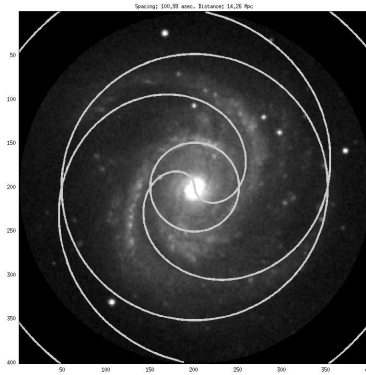


Figure 14: Digital photograph of NGC 4321 with circles overlaid at 100.99 arcsec intervals. The intervals indicate a spacing which matches the pitch of the galaxy. A spiral overlay having a corresponding pitch is also overlaid. It can be seen that the overlaid spiral is as “wound up” as the spiral shown by the brighter regions of the galaxy itself.

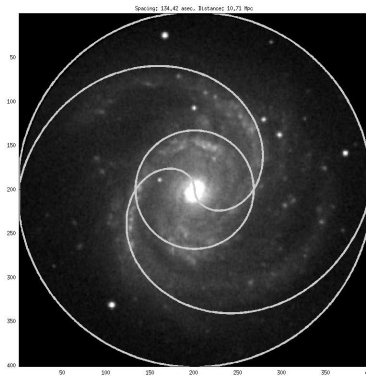


Figure 15: Digital photograph of NGC 4321 with circles overlaid at 134.42 arcsec intervals. The intervals indicate a spacing somewhat larger than the pitch of the galaxy. A spiral overlay having a corresponding pitch is also overlaid. It can be seen that the overlaid spiral is significantly less “wound up” than the spiral shown by the brighter regions of the galaxy itself.

### 4.3 Measuring the Distance to NGC 3198 using Spiral Pitch

In order to apply a model of spiral galaxies as derived in Equation (20), we only require a measure of  $v_{max}$ . The resultant spiral would give us the absolute size of any spiral galaxy. If the distance to the galaxy is known, we can determine the scale. The scale then becomes a distance modulus for galaxies. This distance modulus can be determined by the relationship between  $v_{max}$  and  $\kappa$ . The scale can be determined, independently of distance, by comparing a derived value of  $\kappa$  in units of ly per radian from  $v_{max}$ , and the observed value of  $\kappa$  from digital photographs. This makes the measure of  $\kappa$  the critical parameter in the application of the model to determine the galaxy's distance.

Figure 16 is a photo of NGC 3198 in which the pixels have been transformed to display the galaxy as seen from directly above. The figure was overlaid with a spiral according to Equation (20) using a value of -26 arcsec per radian as a value of  $\kappa$ . This approximates the well-defined spiral portion of NGC 3198. The resultant spiral of this pitch would have an arm spacing of  $\pi \times 26$ , or about 82 arcsec.

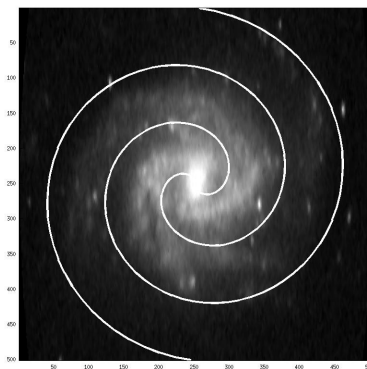


Figure 16: NGC 3198 with spiral overlays according to Equation (20) with a pitch of -26 arcsec per radian.

This property was again investigated by taking 360 luminosity cross sections through the center of the galaxy at half-degree intervals, applying an FFT along these cross sections, and examining the results to see if a value very close to 82 arcsec would appear. A consistent value of 80.83 arcsec presents itself with values of 100.77 and 67.12 arcsec above and below. This analysis is graphically shown in Figures 17 to 20.

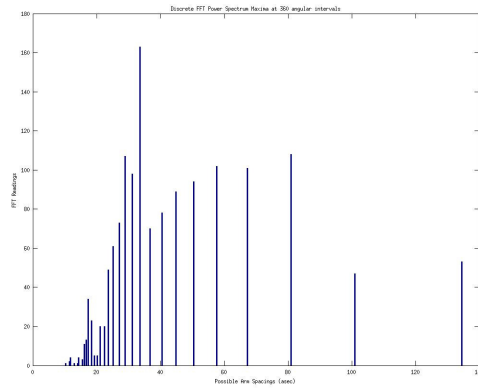


Figure 17: A histogram showing FFT values with different cross section orientations of NGC 3198. A distinct value of 80.83 arcsec can be seen. There are also distinct peaks at 67.12 and 100.77 arcsec to either side.

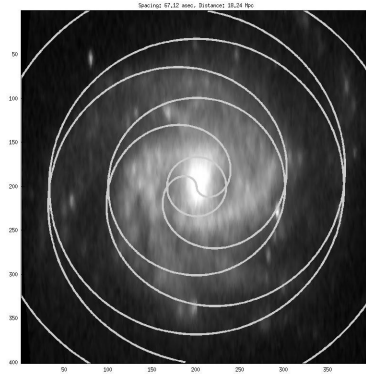


Figure 18: Digital photograph of NGC 3198 with circles overlaid at 67.12 arcsec intervals. The intervals indicate a spacing somewhat smaller than the pitch of the galaxy. A spiral overlay having a corresponding pitch is also overlaid. It can be seen that the overlaid spiral is significantly more “wound up” than the spiral shown by the brighter regions of the galaxy itself.



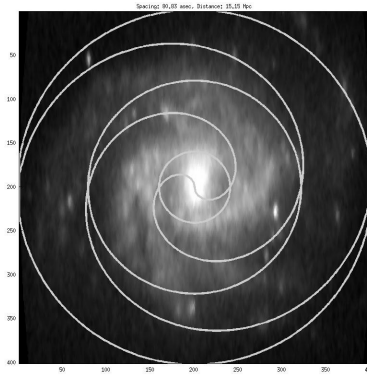


Figure 19: Digital photograph of NGC 3198 with circles overlaid at 80.83 arcsec intervals. The intervals indicate a spacing which matches the pitch of the galaxy. A spiral overlay having a corresponding pitch is also overlaid.

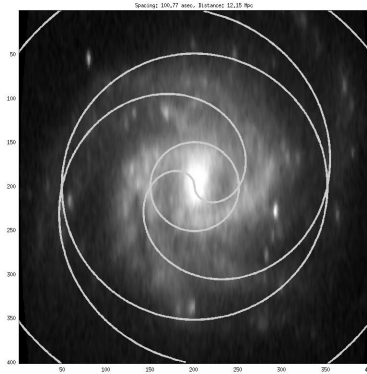


Figure 20: Digital photograph of NGC 3198 with circles overlaid at 100.77 arcsec intervals. The intervals indicate a spacing somewhat larger than the pitch of the galaxy. A spiral overlay having a corresponding pitch is also overlaid. It can be seen that the overlaid spiral is significantly less “wound up” than the spiral shown by the brighter regions of the galaxy itself.

We can validate our model by comparing the predicted intrinsic size of the spiral to the apparent size of a galaxy to estimate its distance. We then compare the derived distance

measure to other distance measures in order to determine a degree of validation for the model. The derived distance modulus is given by the equation:

$$D = \frac{3.12 \times 10^9}{v_{max} \times \alpha_s} \quad (22)$$

where  $3.12 \times 10^9$  is in pc arcmin km/s.

In the case of NGC 3198,  $v_{max}$  is taken as 152.9 km/s based on the above described curve fit of the velocity profile and  $\alpha_s$  is an angular measure of spiral pitch equal to 80.83 arcsec, or 1.347 arcmin. From equation 22 we determine NGC 3198 to be 15.15 ( $\pm 2.5$ ) Mpc distant. The allowable error in  $v_{max}$  is calculated as 7.5 km/s and in  $\alpha_s$  as 0.14 arcmin.

These measurements compare to 13.8 Mpc by Freedman (2001), 12 Mpc using Cepheid variables and 13.8 Mpc using Tully-Fisher by Tully et al. (2008), 10.92 Mpc using redshift by Crook et al. (2007), 14.5 using Cepheid variables by Ferrarese et al. (2000) and 17 Mpc by Gil de Pas et al. (2007).

These measures have a mean of 13.9 Mpc with a standard deviation of 2.0 Mpc of the seven measurements presented here.

## 5 Using Distance Measures to Validate the Model

Distance measures to galaxies can be used to determine a degree of validation for the presented model. There are three different distance measures that will be presented here and compared to predictions. We shall use distance measures using Cepheid variables, the Tully-Fisher relationship and behavior of water masers.

### 5.1 Comparing Distance Measures using Cepheid Variables

We have reviewed distance measurements to galaxies made by Ferrarese et al. (2000) using Cepheid variables (Leavitt, 1908) and compared these measurements to measurements made using equation (22) and rotation curves, (which are cited in Table 4 shown at the end of this paper). Figure 21 is a presentation of a comparison between Cepheid measurements and equation (22) showing a discrepancy from matching a one to one linear fit by 0.016. The confidence variable is 0.9104. Table 4 lists the name of the galaxy in the first column. The second column lists estimates of  $v_{max}$  from rotation curves given by the cited papers below the table with an allowance of 10% as listed in the third column. The fourth column lists the measure of  $\alpha_s$  from an FFT, as described, with the resultant  $\sigma$  of the FFT listed in the fifth. The sixth column lists the distance calculated by equation (22) and the normalized error in the distance measure is listed in the seventh column. The eighth column lists the magnitude difference from observing Cepheid variables within the galaxy and the  $\sigma$  of the measurement in the ninth. The tenth column lists the distance measure calculated from using Cepheid variables and the 11<sup>th</sup> column lists the normalized error in the distance measure using Cepheids. The final column gives references.

From equation (22) the fractional margin of error is the sum of the fractional error in measurement of  $\alpha_s$ , which is given by the FFT used and the fractional error in determining  $v_{max}$ .

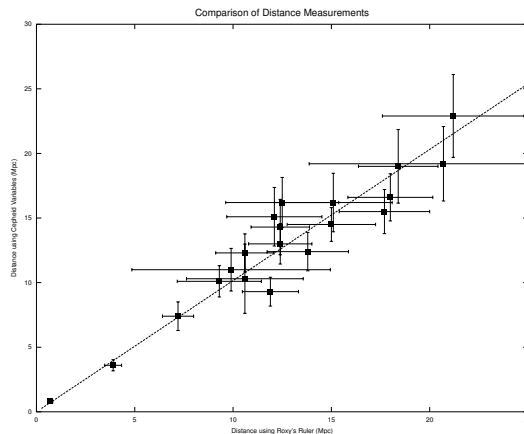


Figure 21: Cepheid distance vs. equation (22) showing a discrepancy from matching a one to one linear fit by 0.016. The confidence variable is 0.9104.

## 5.2 Comparing Distance Measures using Water Masers

Another method to measure the distance to galaxies can be found through the behavior of water masers by Herrnstein et al. (1999). In this method, the magnitudes of orbits of gases containing masers can be measured directly and then compared to the angular measure of these orbits. Herrnstein has measured a distance of  $7.3 \pm 0.3$  Mpc to NGC 4258 using the behavior of water masers within the galaxy while equation (22), yields a distance measure of  $7.1 \pm 0.55$  Mpc. Table 1 contains rotational velocity measurements by Burbidge et al. (1963) which reports that NGC 4258 has dusty regions in which there are no emission patches strong enough to be recorded: “The measures between  $180''$  and  $220''$  on the north west side come from the spiral arm crossed by the spectrograph slit”. A spiral pitch of  $1.81 \pm 0.008$  arcmin and  $v_{max}$  of  $244.0 \pm 17.86$  km/s was used to determine this measure.

---

Table 1: Rotation velocities of NGC 4258 from Burbidge

Distance from center of galaxy (arcsec)	Tangential velocity (km/s)
185	225
188.6	240
192	255
195	255
199.5	255
203.1	255
206.7	240
210.4	270
214	255
217.6	210
221.2	225

---

Data from Burbidge on rotation velocities of NGC 4258 taken from 185'' to 220'' from the center of the galaxy. The data comes from an area of the galaxy where a galactic arm crosses with the major axis. The average is 244.09 km/s with a standard deviation of 17.86 km/s.

Another distance measurement to a galaxy using water maser behavior was conducted by Braatz et al. (2010). Braatz measured the distance to UGC 3789 as  $49.9 \pm 7.0$  Mpc. Unfortunately, no rotation curve for UGC 3789 has been reported for this galaxy. Nevertheless, an H-1 line width is available through NED<sup>1</sup> Theureau et al. (1998), (see Figure 22). Using the spectrum reported for UGC 3789 and reported measurements of the angle of incline of the galaxy,  $44.8^\circ$ , a  $v_{max}$  of  $314.33 \pm 50.7$  km/s was calculated. An FFT across the galaxy's major axis gave a pitch for the galaxy of  $11.99 \pm 0.7$  arcsec. The resultant distance to UGC 3789 using equation (22) is  $49.7 \pm 8$  Mpc.

---

<sup>1</sup>This research has made use of the NASA/IPAC Extragalactic Database (NED) which is operated by the Jet Propulsion Laboratory, California Institute of Technology, under contract with the National Aeronautics and Space Administration.

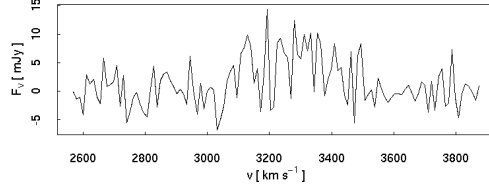


Figure 22: Spectral response of signals traversing the major axis of UGC 3789. The line width is not clear and an estimate of 221.145 km/s from 3063.54 km/s to 3505 km/s is submitted. With an angle of incline of  $44.8^\circ$  yields an estimated  $v_{max}$  of 314.33 km/s.

The measure using equation (22) was particularly difficult to make due to the lack of distinguishing spiral shape of the galaxy. The galaxy is fairly distant and it is tightly wound. Note that its large rotation velocity would result in a tightly wound galaxy in accordance with the model presented here. Furthermore, the spectral line width, as in Figure 22, is somewhat convoluted, and six different measures of the b/a ratio are reported in NED. Therefore, the error allowance is quite large. The average b/a ratio was calculated to be  $0.71 \pm 0.059$ .

### 5.3 Comparing Distance Measures using Tully-Fisher

Yet another method for measuring the distances to galaxies is the well known Tully-Fisher (T-F) (Tully & Fisher, 1977). This method involves an observed relationship between the width of spectral lines and luminosity of spiral galaxies. The spectral line widths are caused by the rotation of the galaxy. This rotational velocity is denoted as  $v_{rot}$  and corresponds to  $v_{max}$ .

In Figure 23, we present a graph of equation (22) measurements vs. distance measurements using T-F. The graph shows a linear fit through the origin with a discrepancy from a one to one match of .0272 and a sigma of 1.38 Mpc. The associated data can be found in Table 2, at the end of this paper. The first column in this table is the name of the galaxy being measured. The second column is the value of  $v_{max}$ . The third column is distance measure using T-F as reported in the Simbad database (U. Strasbourg, 2013). The fourth column is the reported error in the T-F measure in Mpc. The fifth column is the distance measure using equation (22) and the sixth column is the allowable error of the measure in Mpc. The error bars in Figure 23 reflect the reported errors in Table 2.

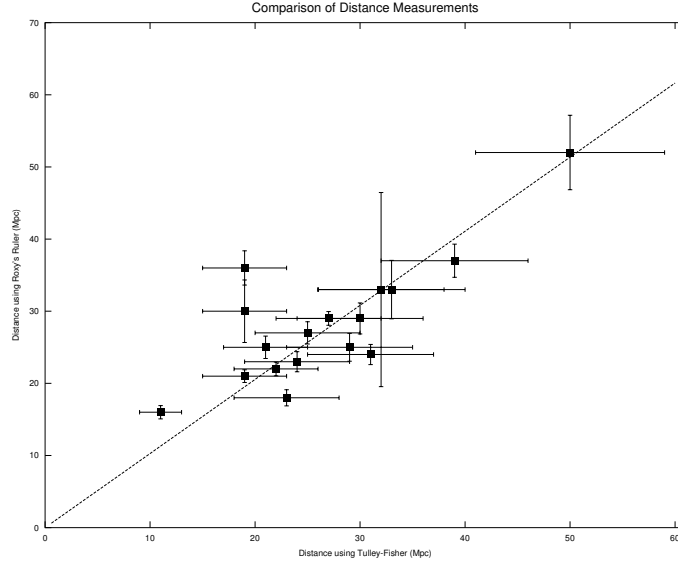


Figure 23: Comparison graph between measures using equation (22) vs Tully-Fisher. The fitted line passes through the origin and has a slope of 1.03 and the fit yields a sigma of 1.38 Mpc.

Table 2: Table of Tully-Fisher Distances

Name	$v_{max}$ (km/s)	T-F Distance (Mpc)	Error (Mpc)	Equation (22) Distance (Mpc)	Error (Mpc)
ESO 284-24	135.073	29	6	25	1.93
ESO 378-11	131.681	50	9	52	5.16
ESO 576-11	146.63	31	6	24	1.40
IC 5078	119.393	19	4	21	0.88
UGCA 17	109.892	23	5	18	1.12
NGC 1090	180.845	27	5	29	0.95
NGC 1163	160.503	39	7	37	2.30
NGC 1337	112.9	11	2	16	0.92
NGC 1832	198.743	25	5	27	1.54
NGC 2763	145.929	24	5	23	1.39
NGC 3321	144.019	33	7	33	4.05
NGC 4348	182.247	30	6	29	2.15
NGC 701	125.347	19	4	30	4.33

Table of Tully-Fisher Distances

Name	$v_{max}$ (km/s)	T-F Distance (Mpc)	Error (Mpc)	Equation (22) Distance (Mpc)	Error (Mpc)
NGC 7218	128.406	21	4	25	1.55
NGC 7339	156.265	22	4	22	0.95
NGC 755	133.339	19	4	36	2.37
NGC 7606	273.5	32	6	33	13.45

Comparisons of distance measures using equation (22) and Tully-Fisher.

Data taken from SIMBAD database operated at CDS, Strasbourg, France

## 6 A Quasi-linear Physical Model

If we project an elongated cloud of stars onto a single dimension, we can map a four dimensional Minkowski space into L-1 space (Minkowski, 1910).

### 6.1 Mass and Linear Density

In the model we are presenting, gravitationally self bound particles appear to be oriented along the path of the spiral shaped geodesic as in equation (20). A mapping of material in  $K'$  into L-1 space through rotation onto a linear axis is straightforward. Using the Lebesgue (1902) measure of linear density in a singular dimension, we have:

$$\rho_l = \frac{v_{max}^2}{G}. \quad (23)$$

Using previously described distance measures and the angular length of the major axis, the intrinsic major axis length,  $L$ , can be determined. Using equation (23) we can determine the mass of the galaxy as:

$$M_g = L\rho_l. \quad (24)$$

From this we can calculate the angular momentum of a galaxy as:

$$l = v_{max}\rho_l L^2. \quad (25)$$

We derive the overall linear density of a galaxy to be within an order of magnitude of  $10^{20}$  kg per meter using Equation (23). The resultant body of particles, in a linear orientation, is highly viscous. Using this linear density, a galaxy having a diameter of 300 million ly would have a mass within an order of magnitude of  $10^{11}$  solar masses.

## 7 CONCLUSIONS

Our calculations take into account Minkowski, Lorentz and Einstein's principles on time and space dilation. We have come to the following conclusions:

## 7.1 Masking Tangential Velocities

Considerations of curvature, relativity, effects of motion, etc. must be thought of locally. Currently, the circular orbital speed of stars within distant galaxies is determined by measuring the shifting of spectral lines of sections of the galaxy. It is not determined by the distance traveled by stars divided by the time it takes for them to get farther along in their orbit. The distances the stars are traveling are vast and we have not observed galaxies for a long enough time to detect circular motion directly. Shifts in spectral lines are not restricted to only the effects of distance traveled divided by time.

In a star's local reference frame, its clocks and rulers differ from the clocks and rulers of other stars in the galaxy due to the variation of the Lorentz transformations at different radial distances from the center. The clocks of each Hydrogen atom in a distant galaxy vary from the clocks of local Hydrogen atoms since the distant orbiting atoms are in a region of curved space and time. Therefore, the shifting of spectral lines of Hydrogen atoms in a distant rotating galaxy is affected by both the Lorentz transformation of Doppler effects and from the Lorentz transformation as a result of the curvature of space-time in a rotating system. Both Lorentz transformations, one varying directly with  $r$  and the other varying inversely, cancel in outer regions of the galaxy and result in the observed constant velocity rotation profile.

We furthermore conclude:

1. General relativity explains the flat velocity rotation profile and morphology of spiral galaxies.
2. Spiral galaxies are gravitationally self bound.
3. Galaxies are gravitationally viscous.
4. Galaxies are morphologically stable.
5. Einstein's general theory of relativity and Newton's principles of gravitational attraction hold over very great distances.

## Acknowledgments

The authors wish to acknowledge the kindness of P. Salucci for access to his data following the loss of the original data tape of Mathewson's observations as a result of a library fire in Australia, the technical assistance of W. Israel, the wide band support of SARA and the encouragement, suggestions and guidance of Roxy.

## References

Abell G. O. 1975, Exploration of the Universe, (3rd ed.: Holt, Rinehart and Winston), 621



- Afanasev V. L., Zasov, A. V., Popravko G. V., & Silchenko O. K. 1991,SvAL,17,325A
- Begeman, K. G. 1989,A&A,223,47
- Binney, J. & Tremain, S. 2008, Galactic Dynamics, Second ed., (Princeton University Press, Princeton, New Jersey),456,480
- Braatz J. A., Reid M. J., Humphreys E. M. L., Henkel C., Condon J. J. & Lo K. Y. 2010,arXiv:astro-ph/1005.1955v1
- Brownstein, J. R., & Moffat, J., W. 2006,ApJ,636,721
- Burbidge, e. M., Burbidge, G. R. & Prendergast, K. H. 1963,ApJ,138,375
- Braine, J, Combes, F & van Driel, W. 1993,A&A,280,451B
- Chemin, L., Cayatte, V., Ballkovski, C., et al. 2003,A&A,405:,89
- Conney, A., Dimitrios, P. & Zaritsky, D. 2012,arXiv:1202.2853v1
- Cooperstock, F. I. & Tieu, S. 2005,arXiv:astro-ph/0507619v1
- Crook A. C., et al. 2007,ApJ,655,790C
- Devereaux, N. A., Kenney, J. D., & Young, J. S. 1992,AJ,103,784D
- Einstein, Albert, Lortntz, H. A., Weyl, H.. Minkowski, H., The Principle of Relativity, (New York, N.Y.:Dover Publications Inc.,1923)
- Ferrarese, L., Ford, H.C., Huchra, J., et al. 2000,ApJS,128,2
- Freedman, W. L. 2001,ApJ,553,47F
- Gallo, C. F. & Feng, J. Q. 2010, J Cosmol,6,1373
- Gil De Pas A.,Boissier S., Madore B. F. et al. 2007,ApJS,173,185G
- Herrnstein J. R., Greenhill L. J., Diamond P. J., et al. 1999,arXiv:astro-ph/9907013v1
- Józsa, G. I. 2007,A&A,468,903
- Kassin, S. A., de Jong, R., & Weiner, B., J. 2006,ApJ,643,804
- Kepler, J. 1619 The Harmony of the World, (self published)
- Knapen,J. H., Shlosman, I., Heller, C. H. ,Rand, R. J. ,Beckman, J. E. & Rozas, M. 2000,ApJ,528,219
- Leavitt, Henrietta S. 1908, Annals of Harvard College Observatory, LX(IV),87,110

- Lebesgue, H. 1902, Intégrale, longueur, aire, (Université de Paris)
- Lindblad, P. A., Lindblad, P. O. & Athanassoula, E. 1996,A&A,313,65
- Mathewson, D. S., Ford, V. L. & Buchhorn, M. 1992,ApJS,81,413
- Menzies, D. & Mathews, G. J. 2006,arXiv:gr-qc/0604092v1
- Minkowski, H 1910, Geometrie der Zahlen, (Leipzig and Berlin)
- Moore, E. M., Gottesman, S. T. 1998,MNRAS,249,353
- Persic, M., Salucci, P., & Fulvio, S. 1995,arXiv:astro-ph/9503051v1
- Pisano, D., J., Wilcots, E., M., & Elmegreen, B., G. 1998,AJ,115,975
- Rohlf, K. & Kreitschmann, J. 1980,A&A,87,175R
- Rubin, V. C. & Ford, W. K. 1970,ApJ,159,379
- Rubin, V. C., Waterman, A., H., & Kenney, J. D., P. 1999,ApJ,118,236
- Mast Phase 2 (GSC2) Survey (2006), <http://archive.stsci.edu/dss/>
- Theureau, G., Bottinelli, L., Coudreau-Durand, N. et al. 1998,A&AS,130,333T
- Tully, R. B., Fisher, J. R. 1977,A&A, 54,3,661
- Tully, R. B. , Shaya E. J., Karachentsev I D., et al. 2008,ApJ,676,184T
- <http://simbad.u-strasbg.fr/simbad/>
- Vallejo, O., Braine, J., & Baudry, A. 2002,A&A,387,429
- Vollmer, B., Cayatte V., Boselli A., Balkowski C., Duschl W.J. 1999,A&A,349,411V
- Woods, D., Fahlman G.G., Madore B.F. 1990,ApJ,353,90
- Youman, Glen 2005, Penryn, California, [www.astrophotos.net](http://www.astrophotos.net), by permission.
- Zwicky, F. 1937,ApJ,86,217Z

## Appendix A Table of Galaxies from Persic & Salucci

Table 3: Table of galaxies from Persic & Salucci.

name	$v_{max}$ ( $ks^{-1}$ )	$\sigma$ (normalized)	name	$v_{max}$ ( $ks^{-1}$ )	$\sigma$ (normalized)	name	$v_{max}$ ( $ks^{-1}$ )	$\sigma$ (normalized)
101-g20	198.9	0.08	120-g16	145.5	0.09	1547-02	209.2	0.03
101-g5	200.4	0.07	123-g15	217.9	0.07	156-g36	151.5	0.36
102-g10	180.7	0.04	123-g16	245.9	0.08	157-g20	143.5	0.03
102-g15	180.3	0.05	123-g23	157.5	0.04	157-g38	91.0	0.12
102-g7	245.2	0.06	123-g9	146.3	0.08	160-g2	217.0	0.15
103-g13	223.2	0.07	124-g15	128.9	0.06	162-g15	86.7	0.11
103-g15	154.6	0.11	13-g16	131.9	0.03	162-g17	65.8	0.03
103-g39	73.6	0.13	13-g18	148.5	0.06	163-g11	168.8	0.04
104-g52	108.3	0.06	140-g24	225.4	0.06	163-g14	180.9	0.09
105-g20	230.6	0.07	140-g25	91.8	0.04	181-g2	296.7	0.12
105-g3	165.7	0.06	140-g28	111.8	0.16	183-g14	141.0	0.07
106-g12	139.0	0.07	140-g33	220.0	0.51	183-g5	97.7	0.06
106-g8	157.0	0.08	140-g34	136.0	0.15	184-g51	262.1	0.04
107-g24	178.6	0.08	140-g43	146.4	0.12	184-g54	186.0	0.09
107-g36	197.2	0.07	141-g20	254.5	0.04	184-g60	88.3	0.11
108-g13	131.6	0.05	141-g23	114.4	0.13	184-g63	178.7	0.07
108-g6	172.8	0.12	141-g34	287.0	0.04	184-g67	231.4	0.06
109-g32	124.6	0.07	141-g37	312.0	0.09	184-g74	206.6	0.20
10-g4	117.6	0.06	141-g9	236.1	0.09	184-g8	128.0	0.19
111-g9	147.0	0.05	142-g30	203.5	0.06	185-g11	230.5	0.08
112-g10	165.0	0.18	142-g35	261.7	0.06	185-g36	176.0	0.04
113-g21	112.1	0.06	143-g10	37.8	0.05	185-g68	114.1	0.06
113-g6	238.1	0.04	143-g6	124.4	0.34	185-g70	153.7	0.08
114-g21	174.6	0.11	143-g8	81.5	0.15	186-g26	77.6	0.07
116-g12	126.8	0.02	145-g18	174.9	0.13	186-g75	123.5	0.06
116-g14	155.6	0.05	145-g22	200.1	0.07	186-g8	134.3	0.07
117-g18	201.0	0.06	146-g6	143.6	0.04	187-g39	114.2	0.08
117-g19	206.6	0.05	151-g30	212.8	0.05	187-g8	138.0	0.04
189-g12	257.0	0.03	231-g6	99.7	0.06	251-g10	238.1	0.11
18-g13	256.2	0.07	233-g36	117.0	0.07	251-g6	170.6	0.06
18-g15	196.6	0.10	233-g41	286.2	0.10	25-g16	131.7	0.10
196-g11	127.9	0.07	233-g42	103.6	0.06	264-g43	260.7	0.08
197-g24	152.5	0.04	234-g13	146.7	0.08	264-g48	178.8	0.08

(Continued...)

Table of galaxies from Persic &amp; Salucci. (Continued)

name	$v_{max}$ ( $ks^{-1}$ )	$\sigma$ (normalized)	name	$v_{max}$ ( $ks^{-1}$ )	$\sigma$ (normalized)	name	$v_{max}$ ( $ks^{-1}$ )	$\sigma$ (normalized)
197-g2	166.0	0.06	234-g32	170.1	0.19	265-g16	158.2	0.05
1-g7	118.4	0.10	235-g16	251.8	0.05	265-g2	57.3	0.05
200-g3	102.4	0.03	235-g20	154.9	0.04	266-g8	106.4	0.03
202-g26	135.8	0.08	236-g37	180.6	0.07	267-g29	198.9	0.11
202-g35	114.1	0.06	237-g15	129.7	0.28	267-g38	223.7	0.09
204-g19	136.7	0.06	237-g49	101.2	0.07	268-g11	232.8	0.11
205-g2	85.1	0.08	238-g24	210.6	0.04	268-g33	230.3	0.05
206-g17	67.7	0.06	239-g17	106.6	0.12	269-g15	242.8	0.06
208-g31	195.7	0.05	240-g11	219.8	0.02	269-g19	177.3	0.02
215-g39	148.6	0.09	240-g13	189.0	0.07	269-g48	99.4	0.11
216-g21	180.4	0.06	241-g21	246.1	0.09	269-g49	140.2	0.11
216-g8	202.8	0.05	242-g18	115.0	0.11	269-g52	193.6	0.04
219-g14	312.6	0.08	243-g14	162.3	0.04	269-g61	369.9	0.07
21-g3	105.6	0.08	243-g34	349.2	0.33	269-g75	110.9	0.06
220-g8	169.0	0.06	243-g36	178.0	0.07	269-g82	125.5	0.15
221-g21	156.0	0.04	243-g8	209.7	0.08	26-g6	116.3	0.04
221-g22	133.5	0.12	244-g31	257.3	0.13	271-g22	180.8	0.05
22-g12	141.4	0.04	244-g43	158.8	0.12	273-g6	236.5	0.08
22-g3	114.7	0.09	245-g10	174.2	0.06	27-g17	215.1	0.06
231-g11	243.1	0.10	249-g16	186.9	0.02	27-g24	188.8	0.06
231-g23	242.9	0.07	249-g35	72.9	0.06	27-g8	176.4	0.06
231-g25	209.0	0.04	24-g19	217.5	0.11	280-g13	276.9	0.10
231-g29	125.4	0.07	250-g17	281.5	0.14	281-g38	212.4	0.08
282-g35	136.7	0.13	303-g14	288.8	0.11	322-g82	213.8	0.04
282-g3	189.0	0.05	304-g16	204.5	0.11	322-g85	111.4	0.10
284-g13	181.5	0.08	305-g14	141.0	0.08	322-g87	152.1	0.09
284-g21	131.2	0.07	305-g6	159.6	0.02	322-g93	108.9	0.11
284-g24	135.1	0.06	306-g2	106.7	0.05	323-g27	201.7	0.09
284-g29	149.5	0.04	306-g32	172.4	0.04	323-g33	146.0	0.07
284-g39	120.8	0.08	308-g23	161.9	0.11	323-g41	152.1	0.08
285-g27	279.3	0.18	309-g17	261.0	0.09	323-g42	129.5	0.10
285-g40	239.5	0.07	309-g5	87.8	0.11	325-g27	104.6	0.12
286-g16	189.5	0.03	30-g9	329.4	0.03	325-g50	89.5	0.06
286-g18	332.7	0.03	310-g2	234.6	0.07	327-g27	120.7	0.09
287-g13	177.5	0.03	317-g32	240.8	0.10	327-g31	129.4	0.04
289-g10	107.5	0.03	317-g52	191.3	0.06	328-g15	203.4	0.07

(Continued...)

Table of galaxies from Persic &amp; Salucci. (Continued)

name	$v_{max}$ ( $ks^{-1}$ )	$\sigma$ (normalized)	name	$v_{max}$ ( $ks^{-1}$ )	$\sigma$ (normalized)	name	$v_{max}$ ( $ks^{-1}$ )	$\sigma$ (normalized)
290-g22	151.1	0.05	319-g16	95.3	0.05	328-g3	227.7	0.05
290-g35	205.0	0.05	319-g26	117.5	0.09	328-g41	238.4	0.05
291-g10	211.4	0.03	31-g18	177.6	0.06	328-g43	107.8	0.05
291-g24	76.9	0.08	31-g5	203.2	0.04	328-g46	240.7	0.07
296-g26	477.4	0.09	320-g24	131.0	0.05	329-g7	270.7	0.05
297-g37	166.6	0.11	320-g26	230.0	0.05	32-g18	207.0	0.06
298-g16	323.2	0.09	320-g2	369.5	0.20	336-g13	194.0	0.05
298-g29	238.6	0.16	321-g10	136.9	0.08	336-g6	264.8	0.19
298-g36	128.8	0.07	321-g17	137.2	0.04	337-g22	145.4	0.07
298-g8	150.1	0.06	321-g1	179.1	0.10	337-g6	188.3	0.09
299-g18	172.7	0.07	322-g33	46.4	0.09	338-g22	119.0	0.05
299-g4	186.2	0.05	322-g36	152.5	0.10	339-g36	162.2	0.05
2-g12	193.9	0.06	322-g45	126.5	0.07	33-g22	185.9	0.07
302-g7	135.2	0.09	322-g48	126.5	0.07	33-g32	177.8	0.09
302-g9	73.6	0.03	322-g55	175.2	0.16	340-g26	169.3	0.04
342-g43	168.7	0.13	354-g47	232.5	0.08	374-g26	135.3	0.08
343-g18	146.5	0.07	355-g26	121.6	0.05	374-g27	253.2	0.04
343-g28	109.4	0.11	356-g15	229.6	0.07	374-g29	133.5	0.08
344-g20	471.6	0.13	356-g18	66.2	0.08	374-g3	145.2	0.04
346-g14	107.9	0.04	357-g16	79.6	0.05	374-g49	211.3	0.06
346-g1	118.0	0.09	357-g19	126.4	0.06	374-g8	71.3	0.06
346-g26	98.4	0.02	357-g3	147.2	0.05	375-g12	283.8	0.10
347-g28	96.0	0.02	358-g17	264.8	0.06	375-g26	171.9	0.03
347-g33	186.6	0.04	358-g58	165.8	0.07	375-g29	175.4	0.05
347-g34	116.9	0.02	358-g63	113.5	0.08	375-g2	182.3	0.11
349-g32	296.4	0.08	358-g9	101.9	0.08	375-g47	143.5	0.12
349-g33	204.7	0.07	359-g6	76.2	0.04	376-g2	233.8	0.09
34-g12	232.6	0.05	35-g18	129.2	0.06	377-g10	193.0	0.05
350-g23	230.5	0.01	35-g3	89.6	0.05	377-g11	341.3	0.10
351-g18	129.4	0.07	361-g12	136.2	0.06	377-g31	175.3	0.06
351-g1	108.2	0.09	362-g11	129.4	0.01	378-g11	131.7	0.06
351-g28	116.7	0.19	363-g23	174.1	0.05	379-g6	176.4	0.05
352-g14	200.9	0.12	363-g7	84.7	0.06	380-g14	185.3	0.11
352-g15	137.6	0.11	365-g28	187.7	0.06	380-g19	239.0	0.04
352-g24	166.2	0.11	365-g31	199.3	0.18	380-g23	113.1	0.05
352-g27	219.1	0.06	366-g4	142.9	0.13	380-g24	154.3	0.08

(Continued...)

Table of galaxies from Persic &amp; Salucci. (Continued)

name	$v_{max}$ ( $ks^{-1}$ )	$\sigma$ (normalized)	name	$v_{max}$ ( $ks^{-1}$ )	$\sigma$ (normalized)	name	$v_{max}$ ( $ks^{-1}$ )	$\sigma$ (normalized)
352-g50	148.7	0.08	366-g9	107.9	0.14	380-g25	66.0	0.17
352-g53	251.4	0.05	36-g19	209.0	0.03	380-g29	87.5	0.37
353-g14	153.9	0.05	373-g12	82.7	0.09	380-g2	54.6	0.07
353-g26	218.2	0.19	373-g21	105.9	0.07	381-g51	249.6	0.06
353-g2	110.7	0.11	373-g29	140.9	0.06	382-g32	225.6	0.12
354-g17	182.8	0.06	374-g10	140.8	0.04	382-g41	95.1	0.10
354-g46	208.1	0.10	374-g11	201.3	0.05	382-g4	170.5	0.09
382-g58	306.7	0.13	406-g26	116.1	0.03	422-g12	340.2	0.10
383-g2	209.3	0.11	406-g33	133.0	0.03	422-g23	248.5	0.19
383-g55	269.1	0.10	40-g12	199.0	0.04	426-g8	176.3	0.04
383-g67	119.4	0.05	410-g19	187.8	0.04	427-g14	97.7	0.09
383-g88	191.0	0.12	410-g27	164.9	0.10	427-g2	210.9	0.03
385-g12	187.5	0.15	411-g3	215.3	0.10	42-g10	173.7	0.05
385-g8	149.8	0.04	412-g15	150.1	0.06	42-g3	239.4	0.04
386-g43	308.8	0.07	412-g21	201.3	0.06	433-g10	163.1	0.09
386-g44	176.3	0.13	413-g14	262.9	0.12	433-g15	126.7	0.05
386-g6	160.4	0.08	413-g23	143.3	0.07	433-g17	365.0	0.11
387-g20	179.2	0.09	414-g25	190.3	0.06	434-g23	145.6	0.07
387-g26	229.4	0.05	414-g8	96.6	0.16	435-g10	138.0	0.05
387-g4	246.6	0.07	415-g10	112.4	0.06	435-g14	170.4	0.08
38-g12	152.9	0.06	415-g15	210.1	0.07	435-g19	101.6	0.09
398-g20	210.0	0.09	415-g28	130.3	0.10	435-g24	183.1	0.07
399-g23	220.4	0.07	416-g37	208.3	0.06	435-g34	135.0	0.05
3-g3	248.7	0.08	416-g41	202.2	0.12	435-g50	124.7	0.06
3-g4	192.2	0.09	417-g18	166.5	0.07	435-g51	130.5	0.09
400-g21	128.8	0.04	418-g15	139.3	0.12	435-g5	326.2	0.08
400-g37	122.5	0.06	418-g1	115.8	0.04	436-g34	271.8	0.07
400-g5	182.8	0.06	418-g8	77.7	0.06	436-g39	215.8	0.06
401-g3	241.5	0.09	418-g9	90.7	0.07	436-g3	162.8	0.03
403-g16	200.4	0.12	419-g3	144.7	0.05	437-g18	126.1	0.12
403-g31	95.7	0.09	419-g4	180.7	0.03	437-g22	149.6	0.07
404-g18	66.7	0.09	41-g6	92.9	0.16	437-g25	159.4	0.06
404-g31	130.3	0.08	41-g9	193.5	0.03	437-g31	136.8	0.14
404-g45	141.2	0.05	420-g3	168.4	0.05	437-g35	103.1	0.10
405-g5	224.1	0.20	422-g10	284.4	0.09	437-g47	78.9	0.07
437-g54	150.0	0.05	444-g86	222.6	0.07	461-g3	243.9	0.08

(Continued...)

Table of galaxies from Persic &amp; Salucci. (Continued)

name	$v_{max}$ ( $ks^{-1}$ )	$\sigma$ (normalized)	name	$v_{max}$ ( $ks^{-1}$ )	$\sigma$ (normalized)	name	$v_{max}$ ( $ks^{-1}$ )	$\sigma$ (normalized)
437-g56	193.3	0.40	445-g19	226.8	0.07	461-g44	186.1	0.09
437-g69	87.8	0.17	445-g26	202.2	0.22	462-g16	118.3	0.06
437-g71	54.8	0.13	445-g39	297.3	0.11	463-g25	243.8	0.04
437-g72	225.9	0.10	446-g18	241.9	0.04	466-g13	204.0	0.09
438-g15	158.5	0.06	446-g1	196.1	0.09	466-g27	229.7	0.13
438-g18	179.3	0.06	446-g23	273.5	0.04	466-g28	165.5	0.07
439-g11	72.3	0.06	446-g2	217.3	0.09	466-g5	133.6	0.07
439-g18	446.8	0.07	446-g44	134.8	0.03	467-g11	302.7	0.06
439-g20	225.7	0.09	446-g51	148.9	0.05	467-g23	223.0	0.07
439-g9	301.5	0.08	446-g53	50.8	0.05	467-g27	196.1	0.06
43-g8	315.1	0.08	446-g58	223.3	0.12	467-g36	200.6	0.08
440-g51	101.8	0.10	447-g19	252.4	0.15	467-g51	92.2	0.04
441-g11	61.5	0.06	447-g21	211.1	0.08	468-g11	178.1	0.05
441-g24	111.4	0.06	447-g23	163.5	0.06	468-g23	95.0	0.02
441-g2	123.5	0.03	448-g13	276.8	0.04	469-g22	186.0	0.22
442-g24	129.4	0.06	44-g13	365.5	0.07	46-g8	99.9	0.08
442-g2	74.0	0.06	44-g1	151.3	0.08	471-g2	240.5	0.14
443-g38	253.2	0.10	450-g18	108.8	0.08	472-g10	146.6	0.08
443-g42	282.4	0.06	452-g8	133.8	0.05	474-g19	126.2	0.17
443-g59	100.7	0.06	459-g14	129.2	0.05	474-g39	179.2	0.06
443-g80	130.2	0.08	459-g6	242.4	0.07	474-g5	133.7	0.04
444-g10	176.4	0.05	460-g25	265.5	0.15	476-g15	150.6	0.02
444-g14	132.1	0.08	460-g29	391.7	0.07	476-g16	211.8	0.08
444-g1	251.3	0.10	460-g31	237.0	0.05	476-g25	188.5	0.09
444-g21	101.9	0.06	460-g8	172.8	0.06	476-g5	266.1	0.08
444-g33	61.0	0.09	461-g10	156.5	0.07	477-g16	108.7	0.05
444-g47	162.1	0.07	461-g25	162.7	0.06	477-g18	196.8	0.06
478-g11	120.9	0.04	490-g36	115.8	0.06	507-g2	159.9	0.09
479-g1	121.9	0.07	490-g45	100.2	0.04	507-g56	210.0	0.06
47-g10	211.3	0.05	496-g19	131.2	0.09	507-g62	164.6	0.07
481-g11	150.4	0.07	497-g14	295.1	0.15	507-g7	299.0	0.04
481-g13	176.1	0.02	497-g18	242.0	0.05	508-g11	112.4	0.03
481-g2	148.7	0.02	497-g34	205.2	0.06	508-g60	152.0	0.06
482-g1	158.5	0.08	498-g3	165.5	0.04	509-g35	211.1	0.09
482-g2	184.8	0.15	499-g22	114.7	0.05	509-g44	258.1	0.10
482-g35	132.0	0.05	499-g26	135.0	0.05	509-g45	130.3	0.04

(Continued...)

Table of galaxies from Persic &amp; Salucci. (Continued)

name	$v_{max}$ ( $ks^{-1}$ )	$\sigma$ (normalized)	name	$v_{max}$ ( $ks^{-1}$ )	$\sigma$ (normalized)	name	$v_{max}$ ( $ks^{-1}$ )	$\sigma$ (normalized)
482-g41	189.6	0.06	499-g39	187.3	0.04	509-g74	158.3	0.04
482-g43	161.8	0.09	499-g4	144.4	0.12	509-g80	260.2	0.21
482-g46	92.2	0.03	499-g5	158.9	0.04	509-g91	136.3	0.04
483-g12	167.6	0.11	4-g19	139.0	0.08	510-g40	134.1	0.05
483-g2	112.8	0.07	501-g11	129.5	0.05	511-g46	120.6	0.07
483-g6	175.4	0.04	501-g1	156.5	0.09	512-g12	186.7	0.07
484-g25	157.7	0.17	501-g68	154.5	0.10	514-g10	161.8	0.07
485-g12	152.7	0.05	501-g69	92.1	0.05	51-g18	96.5	0.05
485-g4	145.2	0.04	501-g75	167.5	0.04	526-g11	134.5	0.08
487-g19	99.1	0.06	501-g80	71.8	0.04	527-g11	220.7	0.09
487-g2	177.8	0.04	501-g86	172.9	0.15	527-g19	219.5	0.09
488-g44	117.6	0.08	501-g97	267.9	0.08	527-g21	132.5	0.10
488-g54	180.8	0.04	502-g12	151.0	0.07	528-g17	140.3	0.09
489-g11	140.1	0.06	502-g13	132.7	0.01	528-g34	165.3	0.10
489-g6	117.1	0.05	502-g2	206.0	0.07	530-g34	223.8	0.08
48-g8	224.4	0.03	505-g8	81.1	0.16	531-g22	182.2	0.03
490-g10	135.7	0.06	506-g2	234.6	0.04	531-g25	177.2	0.05
490-g14	116.6	0.05	506-g4	355.0	0.07	532-g14	62.5	0.06
490-g28	55.2	0.07	507-g11	213.6	0.09	533-g48	151.3	0.05
533-g4	170.1	0.04	547-g14	243.4	0.05	554-g28	118.2	0.09
533-g53	163.6	0.01	547-g1	96.2	0.07	554-g29	129.8	0.05
533-g8	175.8	0.08	547-g24	120.0	0.05	554-g34	177.3	0.04
534-g24	157.3	0.08	547-g31	160.0	0.06	555-g16	258.1	0.04
534-g31	282.6	0.07	547-g32	195.4	0.08	555-g22	100.2	0.03
534-g3	167.3	0.15	547-g4	124.9	0.13	555-g29	132.9	0.07
534-g9	226.4	0.06	548-g21	66.3	0.07	555-g2	143.9	0.07
535-g15	212.9	0.08	548-g31	190.9	0.05	555-g8	138.9	0.08
536-g17	175.9	0.16	548-g32	63.9	0.04	556-g12	106.4	0.17
539-g14	155.7	0.07	548-g50	77.5	0.07	556-g23	148.7	0.05
539-g5	156.0	0.06	548-g63	104.5	0.09	556-g5	166.0	0.07
53-g2	159.9	0.08	548-g71	80.6	0.09	55-g29	169.4	0.12
540-g10	120.7	0.13	548-g77	87.1	0.08	55-g4	245.6	0.03
540-g16	80.0	0.04	549-g18	168.6	0.06	55-g5	78.4	0.19
541-g1	247.0	0.07	549-g22	134.2	0.08	562-g14	199.9	0.04
541-g4	147.8	0.04	549-g40	273.2	0.06	563-g11	269.5	0.08
543-g12	162.2	0.04	54-g21	109.3	0.07	563-g13	182.6	0.05

(Continued...)



Table of galaxies from Persic &amp; Salucci. (Continued)

name	$v_{max}$ ( $ks^{-1}$ )	$\sigma$ (normalized)	name	$v_{max}$ ( $ks^{-1}$ )	$\sigma$ (normalized)	name	$v_{max}$ ( $ks^{-1}$ )	$\sigma$ (normalized)
544-g27	159.2	0.07	550-g7	67.8	0.02	563-g14	148.3	0.02
544-g32	145.1	0.07	550-g9	186.3	0.06	563-g17	244.5	0.07
545-g11	191.3	0.02	551-g13	161.9	0.12	563-g21	356.0	0.03
545-g21	184.0	0.05	551-g16	49.1	0.07	563-g28	193.8	0.09
545-g3	40.6	0.07	551-g31	72.1	0.07	564-g20	81.6	0.04
545-g5	96.6	0.03	552-g43	181.7	0.13	564-g23	175.9	0.05
546-g15	310.4	0.09	553-g26	205.0	0.06	564-g31	171.0	0.06
546-g29	157.3	0.03	553-g3	260.8	0.08	564-g35	109.8	0.04
546-g31	207.4	0.05	554-g10	268.0	0.03	566-g14	179.2	0.07
546-g36	188.1	0.09	554-g19	145.9	0.07	566-g22	136.5	0.03
546-g37	119.1	0.09	554-g24	129.5	0.05	566-g26	188.9	0.04
566-g30	156.4	0.06	576-g51	167.0	0.04	58-g3	148.8	0.13
566-g9	156.0	0.10	577-g1	176.4	0.11	593-g3	186.1	0.05
567-g26	202.7	0.04	579-g25	165.5	0.17	594-g8	186.4	0.07
567-g45	292.9	0.12	579-g9	114.7	0.07	595-g10	132.0	0.05
567-g6	98.2	0.07	57-g80	159.1	0.05	596-g9	126.0	0.11
568-g19	189.7	0.22	580-g29	159.3	0.05	59-g23	169.5	0.05
569-g22	220.4	0.05	580-g37	199.7	0.12	59-g24	252.5	0.04
570-g2	154.2	0.06	580-g41	104.1	0.05	601-g19	193.4	0.09
571-g12	175.8	0.18	580-g45	130.5	0.06	601-g25	74.9	0.07
571-g15	235.4	0.07	580-g49	134.9	0.06	601-g4	160.1	0.06
571-g16	152.1	0.08	580-g6	160.8	0.05	601-g5	157.2	0.09
572-g18	139.4	0.06	581-g10	126.6	0.12	601-g7	105.0	0.13
572-g22	81.9	0.08	581-g11	188.0	0.11	601-g9	291.0	0.02
572-g49	87.0	0.05	581-g15	173.5	0.11	602-g15	79.7	0.07
573-g14	144.2	0.08	581-g4	120.4	0.07	602-g25	202.6	0.10
573-g6	135.7	0.08	581-g6	118.6	0.09	603-g12	101.0	0.04
574-g28	129.3	0.07	582-g12	166.8	0.06	603-g20	110.3	0.06
574-g32	163.4	0.09	582-g13	245.6	0.11	603-g22	268.8	0.05
574-g33	184.7	0.08	582-g1	230.3	0.32	604-g1	75.6	0.06
575-g53	135.3	0.06	582-g21	214.6	0.07	605-g7	106.7	0.05
576-g11	146.6	0.04	582-g4	99.6	0.10	606-g11	174.1	0.09
576-g12	158.1	0.10	583-g2	208.3	0.06	60-g15	98.5	0.05
576-g14	194.8	0.04	583-g7	398.2	0.07	60-g24	286.0	0.47
576-g26	76.0	0.05	584-g4	211.2	0.07	60-g25	41.2	0.10
576-g32	172.5	0.08	586-g2	119.8	0.07	61-g8	146.5	0.05

(Continued...)

Table of galaxies from Persic &amp; Salucci. (Continued)

name	$v_{max}$ ( $ks^{-1}$ )	$\sigma$ (normalized)	name	$v_{max}$ ( $ks^{-1}$ )	$\sigma$ (normalized)	name	$v_{max}$ ( $ks^{-1}$ )	$\sigma$ (normalized)
576-g39	156.9	0.07	58-g25	198.8	0.06	62-g3	145.1	0.06
576-g3	92.6	0.05	58-g28	76.3	0.08	69-g11	164.0	0.05
576-g48	231.0	0.07	58-g30	177.8	0.04	6-g3	163.0	0.05
71-g14	219.8	0.04	8-g7	152.9	0.05	m-2-2502	167.3	0.04
71-g4	116.9	0.07	90-g9	173.5	0.06	m-2-2-51	278.8	0.10
71-g5	235.8	0.06	9-g10	179.2	0.04	m-2-7-10	130.1	0.05
72-g5	140.4	0.08	holm370	186.9	0.04	m-2-7-33	188.3	0.04
73-g11	218.6	0.07	i1330	225.2	0.07	m-2-8-12	187.6	0.06
73-g22	202.1	0.05	i1474	147.2	0.06	m-3-1042	149.8	0.03
73-g25	145.4	0.07	i2974	238.0	0.03	m-3-1364	165.4	0.04
73-g42	135.5	0.24	i382	201.2	0.05	m-3-1623	196.1	0.05
74-g19	186.9	0.09	i387	248.1	0.12	m-338025	163.0	0.04
75-g37	130.9	0.03	i407	189.2	0.04	n1090	180.8	0.03
79-g14	154.7	0.02	i416	117.9	0.03	n1114	195.3	0.04
79-g3	252.4	0.02	i5078	119.4	0.03	n1163	160.5	0.06
7-g2	152.6	0.15	i5282	207.8	0.08	n1241	282.6	0.07
80-g1	110.8	0.10	i784	191.5	0.05	n1247	268.8	0.03
82-g8	263.0	0.06	i96099	176.1	0.02	n1337	112.9	0.03
84-g10	198.8	0.02	m-1-1035	191.4	0.03	n1417	235.1	0.10
84-g33	288.8	0.04	m-1-2313	158.1	0.04	n1421	170.0	0.19
84-g34	235.2	0.35	m-1-2321	180.5	0.05	n151	325.5	0.05
85-g27	179.2	0.07	m-1-2522	170.1	0.05	n1620	214.0	0.05
85-g2	197.5	0.04	m-1-2524	77.5	0.04	n1752	224.3	0.04
85-g38	178.3	0.06	m-1-5-47	226.0	0.03	n1832	198.7	0.03
85-g61	94.5	0.06	m-2-1009	258.0	0.04	n2584	187.3	0.06
87-g3	283.8	0.16	m-213019	166.5	0.06	n2721	242.7	0.05
87-g50	97.9	0.07	m-214003	150.6	0.04	n2722	134.9	0.05
88-g16	201.4	0.04	m-215006	129.9	0.06	n2763	145.9	0.03
88-g17	350.1	0.15	m-222023	299.8	0.06	n280	319.8	0.05
88-g8	203.9	0.13	m-222025	159.8	0.15	n2980	234.4	0.04
8-g1	113.3	0.08	m-2-2-40	166.1	0.06	n3029	170.4	0.13
n3138	183.0	0.05	n755	133.3	0.03	u12571	184.4	0.05
n3321	144.0	0.07	n7568	224.0	0.05	u12583	105.4	0.05
n3361	136.2	0.04	n7593	141.5	0.06	u14	198.0	0.05
n3456	168.0	0.05	n7606	273.5	0.30	u1938	188.2	0.05
n3715	193.2	0.06	n7631	205.2	0.06	u2020	90.0	0.06

(Continued...)

Table of galaxies from Persic & Salucci. (Continued)

name	$v_{max}$ ( $ks^{-1}$ )	$\sigma$ (normalized)	name	$v_{max}$ ( $ks^{-1}$ )	$\sigma$ (normalized)	name	$v_{max}$ ( $ks^{-1}$ )	$\sigma$ (normalized)
n4348	182.2	0.03	n7677	181.7	0.11	u2079	125.5	0.05
n4705	195.7	0.02	u12123	118.9	0.06	u210	111.3	0.06
n697	197.2	0.02	u12290	240.0	0.05	u321	79.8	0.07
n699	200.9	0.04	u12370	116.8	0.09	u541	118.2	0.07
n701	125.3	0.11	u12382	124.0	0.10	ua17	109.9	0.02
n7218	128.4	0.02	u12423	262.6	0.07			
n7300	244.7	0.03	u12533	253.8	0.04			
n7339	156.3	0.02	u12555	114.8	0.07			
n7536	183.6	0.04	u12565	186.3	0.09			

This table lists fitted  $v_{max}$  and normalized  $\sigma$  of fit.

Index to names are n: NGC, m: Messier, i: IC, u:UGC, holme: Holmberg, others are ESO numbers.

## Appendix B Comparison of Distance Measures: Spiral Morphology vs Cepheid Variables

Table 4: Comparisons of distance measures using equation (22) and Cepheid Variables.

Name	$v_{max}$ km/s	Error km/s	$\alpha$ (arcmin)	$\sigma$	Equ (22) distance (Mpc)	Norm. Error	m-M	$\sigma$	Cepheid distance (Mpc)	Norm. Error	Ref
NGC 7331	225	22.5	1.15	0.096	12.1	0.20	30.89	0.1	15.1	0.15	1
NGC 3319	130	13	1.94	0.017	12.4	0.12	30.78	0.1	14.3	0.15	2
NGC 4321	130	13	1.68	0.056	14.26	0.16	31.04	0.09	16.2	0.14	3
NGC 4414	230	23	0.66	0.227	20.7	0.33	31.41	0.1	19.2	0.15	4,5
NGC 224	241	24.1	18.94	0.090	.7	0.19	24.44	0.1	.8	0.15	6
NGC 3627	190	19	1.55	0.181	10.6	0.28	30.06	0.17	10.3	0.26	7
NGC 4536	125	12.5	1.41	0.031	17.7	0.13	30.95	0.07	15.5	0.11	8
NGC 3031	140	14	5.77	0.005	3.9	0.11	27.8	0.08	3.6	0.12	9
NGC 3351	220	22	1.53	0.130	9.3	0.23	30.01	0.08	10.1	0.12	10
NGC 2090	150	15	1.96	0.043	10.6	0.14	30.45	0.08	12.3	0.12	11
NGC 4548	157	15.7	1.59	0.132	12.5	0.23	31.04	0.08	16.2	0.12	12
NGC 925	120	12	2.18	0.024	11.9	0.12	29.84	0.08	9.3	0.12	13
NGC 3198	153	15.1	1.35	0.046	15.15	0.15	30.8	0.06	14.5	0.09	14
NGC 4639	200	20	0.73	0.075	21.2	0.17	31.8	0.09	22.9	0.14	15
NGC 4725	210	21	1.2	0.028	12.4	0.13	30.57	0.08	13.0	0.12	16
NGC 3368	220	22	1.44	0.410	9.9	0.51	30.2	0.1	11.0	0.15	16
NGC 5457	190	19	2.29	0.009	7.2	0.11	29.34	0.1	7.4	0.15	16
NGC 598	130	13	33.8	0.001	.7	0.10	24.64	0.09	.8	0.14	16,17
NGC 4535	140	14	1.24	0.022	18.0	0.12	31.1	0.07	16.6	0.11	17
NGC 1365	50	5	3.4	0.012	18.4	0.11	31.39	0.1	19.0	0.15	18
NGC 2541	95	9.5	2.39	0.052	13.8	0.15	30.47	0.08	12.4	0.12	19

References. (1) Rubin & Ford (1970); (2) Moore & Gottesman (1998);  
(3) Knapen et al. (2000); (4) Braine & van Driel (1993);  
(5) Vallejo et al (2002); (6) Abell (1975);  
(7) Chemin et al. (2003); (8) Afanasev et al. (1991);  
(9) Rohlfs & Kreitschmann (1980); (10) Devereaux et al. (1992);  
(11) Kassin et al. (2006); (12) Vollmer et al. (1999);  
(13) Pisano et al. (1998); (14) Begeman (1989);  
(15) Rubin et al. (1999); (16) Brownstein & Moffat (2006);  
(17) Woods et al. (1990); (18) Lindblad et al. (1996);  
(19) Józsa (2007)

